IEEE Access
Multidisciplinary ⋮ Rapid Review ⋮ Open Access Journal

Received June 17, 2021, accepted July 12, 2021, date of publication July 26, 2021, date of current version July 30, 2021.

Digital Object Identifier 10.1109/ACCESS.2021.3099772

Visible Light Communication for Connected Vehicles: How to Achieve the Omnidirectional Coverage?

HOSSIEN B. ELDEEB[1], (Graduate Student Member, IEEE), SADIQ M. SAIT[2], (Senior Member, IEEE), AND MURAT UYSAL[1], (Fellow, IEEE)

[1]Department of Electrical and Electronics Engineering, Özyeğin University, 34794 Istanbul, Turkey
[2]Center for Communications and IT Research, Department of Computer Engineering, Research Institute, King Fahd University of Petroleum and Minerals, Dhahran 31261, Saudi Arabia

Corresponding author: Hossien B. Eldeeb (hossien.eldeeb@ozyegin.com)

This work was supported by the Horizon 2020 MSC ITN (VISION) under Grant 76446. The work of Murat Uysal was supported by the Turkish Scientific and Research Council (TUBITAK) under Grant 215E311. The work of Sadiq M. Sait was supported by the King Fahd University of Petroleum and Minerals (KFUPM) Deanship of Scientific Research under Project SB191038.

ABSTRACT Visible light communication (VLC) is based on the idea of modulating the light intensity of LEDs to transmit information and enables the dual use of exterior automotive and road side infrastructure lighting for both illumination and communication purposes. To position VLC as a strong candidate for vehicular connectivity, it is essential to realize multi-directional reception in various deployment scenarios supporting both vehicle-to-vehicle (V2V) and infrastructure-to-vehicle (I2V) links. In this paper, we investigate the performance of a vehicular VLC system in different road types (i.e., multi-lane, curved roads), intersections (i.e., T-shaped, Y-shaped intersections) and traffic scenarios (i.e., cruising in the same or different lanes, lane change etc.). We conduct a channel modeling study based on non-sequential ray tracing to quantify the capability of receiving signals in different cases. Our results reveal that deployment of nine photodetectors with carefully determined locations on the vehicle is enough to create the required quasi-omni-directional coverage for both V2V connectivity (in front and back directions) and I2V connectivity.

INDEX TERMS Vehicular visible light communications, connected vehicle, omni-directional coverage, multi-lane road, curved road, intersections, receiver model.

I. INTRODUCTION

Vehicular communication is one of the key enabling technologies for future intelligent transportation systems (ITSs) [1], [2]. It allows the vehicles to share information with each other and with infrastructures along the road. While vehicle-to-vehicle (V2V) links are particularly important for safety functionalities such as pre-crash sensing and forward collision warning, infrastructure-to-vehicle (I2V) links provide the connected vehicles with a variety of useful information (e.g., traffic density, alternative routes, services along the road etc.) [3]. The earlier works on vehicular communication have mainly focused on radio frequency (RF) technologies [4]–[7]. The widespread utilization of light emitting diode (LED)-based headlights (HLs), taillights (TLs), street lights, and traffic lights in vehicles and road side infrastructures has further prompted the investigation of visible light communication (VLC) as a potential candidate for vehicular connectivity [8]–[12]. VLC is based on the idea of modulating the light intensity of LEDs to transmit information and enables the dual use of exterior automotive and infrastructure lighting for both illumination and communication purposes [13], [14].

There is already a growing number of works on V2V [15]–[31] and I2V [32]–[38] VLC systems. An overview of existing works on V2V and I2V can be found in Table 1 and Table 2, respectively. As can be checked from Table 1 that the common underlying assumption in V2V works is the use of one or two photodetectors (PDs) placed at the back of the vehicle [15]–[26]. This is typically sufficient for establishing connection between two vehicles cruising in the same straight lane with no or small horizontal displacement between each other. To ensure reception in wider roads (i.e., two-lane) and curved roads, more PDs are typically

The associate editor coordinating the review of this manuscript and approving it for publication was Qing Yang.

TABLE 1. Overview of existing V2V works.

Ref	TX	No. PDs	Road shape	Description
[15]	HLs	1 PD	Straight road (Single lane)	A V2V system in a straight road and in one direction was considered assuming a perfect alignment between the vehicles, i.e., d_h = 0 m.
[16, 17]	TL	1 PD	Straight road (Single lane)	A V2V system in straight road was considered where a measured car TL pattern was integrated into a ray tracing platform to investigate the channel path loss using single PD. The perfect alignment between the vehicles was assumed, i.e., d_h = 0 m.
[18]	TL	1 PD	Straight road (Single lane)	The performance of a V2V system was investigated utilizing an off-the-shelf scooter taillight as the transmitting end and a single PD as the receiver one. A lateral shift of $d_h \approx w_l/2$ was considered.
[19]	HLs	1 PD	Straight road (Single lane)	A V2V communication system in a straight road and one direction was considered. A lateral shift of $d_h \approx w_l/2$ was assumed.
[20]	HLs	1 PD	Straight road (Two-lane)	The time variation of V2V VLC channels was investigated in freeway and urban areas by low beam headlamp and a single PD.
[21]	HLs	1 PD	Straight road (Two-lane)	A V2V communication system in a straight road and in one direction was considered with a possible lateral shift of $d_h \approx w_l/2$.
[22]	HL	1 PD	Straight road Two-lane & Turning path	A V2V system in straight and turning path roads was considered. A low beam HL and a single PD were utilized to investigate the effect of using different lens combinations on the system performance.
[23]	HLs	1 PD	Straight road (Three-lane)	A V2V system in a three-lane road and in one direction was considered utilizing a low beam tungsten lamp and a single PD.
[24]	HLs	1 PD	Straight road (Three-lane)	A V2V communication system in a three-lane road and in one direction was considered. A possible lateral shift of $d_h \approx w_l/2$ was considered. The performance of three commercial low beam modules and two high beams are investigated and compared.
[25]	HLs	12 PDs	Straight road (Single lane)	A V2V system in a straight road and only in one direction was considered. Two PDs were combined using EGC scheme to improve the system performance assuming a perfect alignment, i.e., d_h = 0 m.
[26]	White LED	2 PDs	Straight road (Single lane)	A V2V system in a straight road and one direction was considered. A phosphor-based white LED was used assuming Lambertian pattern for headlight where two PDs were combined using MRC scheme.
[27]	HL & TL	2 PDs	Straight road (Three-lane)	A V2V system in three lane straight road was considered. The HL and TL of the vehicle were utilized to achieve the connectivity in the front and back directions where for each link one PD was utilized to receive the signal. A lateral shift of $d_h \approx w_l/2$ was considered.
[28]	HL & TL	2 PDs	Straight road Three-lane & Turning path	A V2V system in a three-lane road was considered. HLs and TLs of the vehicle were used to achieve the communication in two directions. Also, the impact of the turning path on system performance was emphasized. It was observed a high outage ratio in the turning path road comparing to the straight one assuming a single PD.
[29]	White LED	3 PDs	Straight road Two-lane & Turning path	A V2V system was considered in a straight and a turning path assuming one direction communication. In which, a white LED (with Lambertian pattern) was utilized to represent the headlight and three PDs were combined with different combining schemes.
[30]	HLs	4 PDs	Straight road (Single lane)	A V2V communication system in straight road and one direction was considered. An ADR, consists of four PDs, was utilized to improve the system performance.
[31]	HLs	4 PDs	Straight road (Two-lane)	A V2V system in a straight road and in one direction was considered. Two vehicles follow each other in same lane or different lanes. Four PDs were distributed around the back and the side of the vehicle to achieve the omni-directional coverage in such practical cases.

TABLE 2. Overview of existing I2V works.

Ref	TX	No. PDs	Road shape	Description
[32]	Array of WLEDs	1 PD	Straight road (Single lane)	An I2V system is realized by using array of WLEDs to fit with standard traffic light and a single PD act as a receiver. The channel path loss over the distance was calculated where about 42 dB was the recorded attenuation value at 100 m assuming a perfect alignment, i.e., $d_h = 0$ m.
[33]	Commercial -off-the-shelf LED	1 PD	Straight road (Single lane)	An I2V communication system in a straight road was considered. The optical channel path loss between LED traffic light and vehicles was investigating utilizing the commercial-off-the-shelf LED and a single PD where a perfect alignment was assumed, i.e., $d_h = 0$ m.
[34]	Streetlight	1 PD	Straight road (Single lane)	A comparison between VL, IR, and UV bands in I2V based streetlight system with perfect alignment, i.e., $d_h = 0$ m. In which, the UV band is the worst case in terms of SNR.
[35]	Traffic light	1 PD	Straight road (Single lane)	A hybrid I2V-V2I VLC system was investigated in a single lane straight road. A regular LED traffic light, was used as a transmitter and a single PD was used as a receiver with perfect alignment, i.e., $d_h = 0$ m.
[36]	Traffic light	1 PD	Straight road (Single lane)	An I2V VLC system was investigated in a single lane straight road. A regular LED traffic light, was used as a transmitter and a single PD was used as a receiver with perfect alignment, i.e., $d_h = 0$ m.
[37]	White LED	1 PD	Straight road (Two-lane)	An I2V communication system in a straight road was considered. In which, a white LED was utilized to represent the streetlight lamp and a single PD acted as a receiver where a channel estimation method was proposed.
[38]	Streetlight	1 PD	Straight road (Two-lane)	An I2V communication system based commercial streetlights in a straight road and with possible lateral shift of $d_h \approx w_l/2$ was considered. In which, the effect of the nearby cars same as car velocity on the received SNR were investigated

required. For example, in [29], three PDs are deployed and, among three PDs, the one with maximum received power is chosen. In [30], the performance of the V2V system is investigated utilizing an angle diversity receiver consisting of 4 PDs oriented in different directions. In [31], four PDs are used to prevent outages of a V2V system during lane change in a two-lane straight road.

As seen from Table 2, most of the I2V works [32]–[38] assume a single PD. Some of these [32], [35], [36] assume PD location at the front hood of the vehicle which is typically favorable for reception from traffic light while some [34], [37], [38] consider the top of the vehicle which is more suitable for reception from street lights. Such a single PD use can be justified in a single lane road with clear line-of-sight between the vehicle and the road side infrastructure.

In addition to aforementioned works which focus only on V2V and I2V links, there have been some sporadic efforts how to enable both V2V and I2V reception. In [39], a receiver located at the vehicle's rooftop is utilized to receive the signals from the infrastructure and from the TLs of the front vehicle. In [40], four PDs are utilized; the PD located at the top of the vehicle is used for the reception from the infrastructure while three PDs, located at the back of the vehicle, are used to receive the signals from the HLs of the following vehicle. These works, however, are limited to simple scenarios where two vehicles follow each other in single-lane or two-lane straight roads.

To position VLC as a strong candidate for vehicular connectivity, it is essential to realize multi-directional reception in various deployment scenarios supporting both V2V and I2V links. It remains an open question what is the sufficient number of required PDs to achieve this. To address this question of practical relevance, we investigate the performance of a vehicular VLC system in different road types (i.e., multi-lane and curved roads), intersections (i.e., T-shaped and Y-shaped intersections) and traffic scenarios (i.e., cruising in the same or different lanes, lane change etc.). We conduct a channel modeling study based on non-sequential ray tracing to quantify the capability of receiving signals in different cases. We first quantify the total received power versus distance for different scenarios under consideration. Our results reveal that deployment of nine PDs with carefully determined locations on the vehicle is sufficient to create the required quasi-omni-directional coverage for both V2V connectivity (in front and back directions) and I2V connectivity. Then, we quantify the contribution of individual PDs to elaborate the main usage cases of each PD. We further investigate the effect of neighbor vehicles and possible blockage on the system performance. To the best of our knowledge, such a comprehensive study on vehicular VLC channel modelling with multiple receive apertures is not available in the literature.

The remainder of this paper is organized as follows. In Section II, we describe our system model and vehicular scenarios under investigation. In Section III, we explain the main steps of our channel modelling approach. In Section IV, we present the simulation results to quantify the total received power versus distance for different scenarios under

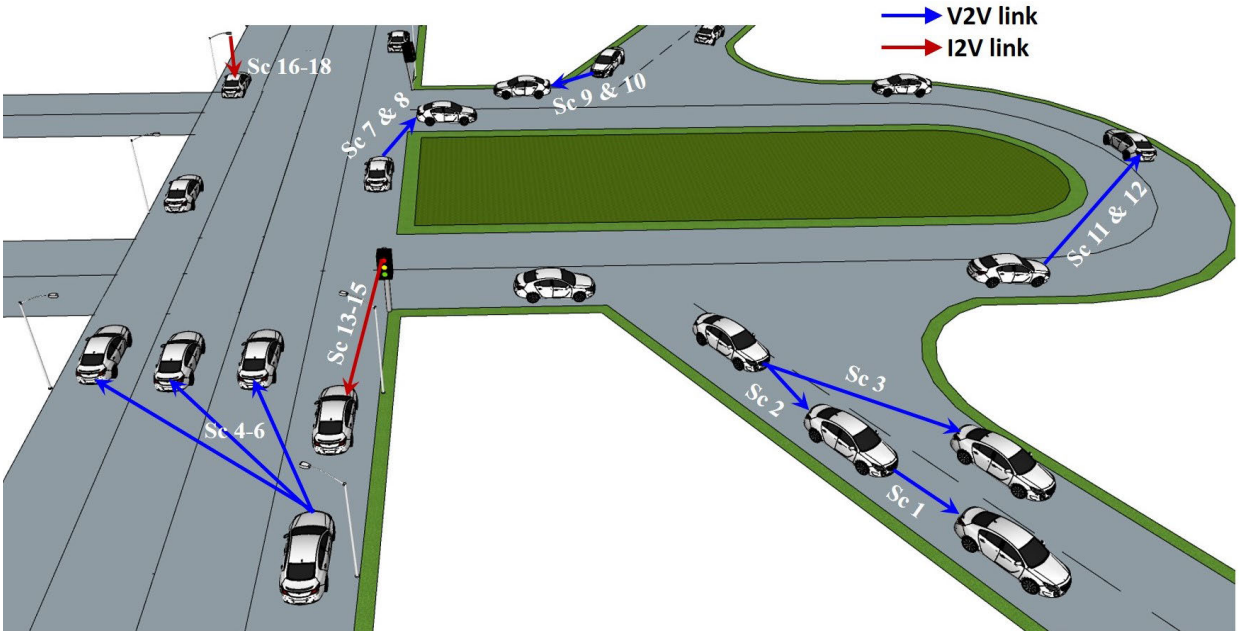

FIGURE 1. Vehicular VLC scenarios under consideration.

consideration. We further quantify the contribution of individual PDs to elaborate the main usage cases of each. Finally, we conclude in Section V.

II. SYSTEM MODEL AND VEHICULAR SCENARIOS

Since the focus of our paper is to investigate the placement and the number of PDs, we only consider the destination vehicle in V2V and I2V links. As illustrated in Fig.1, the destination vehicle can receive signals from the front vehicle (where the TLs of the front vehicle serve as the transmitters) or from the preceding vehicle (where the HLs of the preceding vehicle serves as the transmitters). In I2V links, the wireless transmitters are street lights or traffic lights. The scenarios under consideration are summarized in Table 3. We consider V2V links in two-lane roads (Scenarios 1-3), multi-lane roads (Scenarios 4-6), T-shaped intersections (Scenarios 7 and 8), Y-shaped intersections (Scenarios 9 and 10), and curved roads (Scenario 11 and 12). We consider I2V links either with traffic lights (Scenarios 13-15) or street lights (Scenarios 16-18). In the above scenarios, we have focused on cases where there are no neighbor vehicles or blockage nearby. Finally, in Scenarios 19-21, we investigate the effect of neighbors and possible blockage due to other vehicles in the same lane.

In Scenarios 1-3, we consider a straight road with two lanes each of which has a width of w_l. The vehicles are separated with a longitudinal distance of d and a horizontal distance of d_h

- **Scenario 1 (Fig. 2.a):** In this ideal scenario widely assumed in the literature, the vehicles follow each other in the same lane and with a perfect alignment, i.e., $d_h = 0$.
- **Scenario 2 (Fig. 2.b):** The vehicles follow each other in the same lane but there is a misalignment between the vehicles. The maximum lateral shift between the two vehicles is $d_h = w_l - w_v$ where w_l denotes the width of the vehicle.
- **Scenario 3 (Fig. 2.c):** The two vehicles move in neighbor lanes and the source vehicle changes its lane approaching to the destination vehicle within the target lane.

In Scenarios 4-6, we consider a multi-lane road where each lane has a width of w_l.

- **Scenario 4 (Fig. 2.d):** The source vehicle, located at the center of the 1^{st} lane, communicates with a destination vehicle that travels at the center of the 2^{nd} lane. This creates a lateral shift of $d_h = w_l$ between source and destination vehicles.
- **Scenario 5 (Fig. 2.e):** The source vehicle cruising at the center of the 1^{st} lane, communicates with a destination vehicle cruising at the center of the 3^{rd} lane, effectively resulting in a lateral shift of $d_h = 2w_l$.
- **Scenario 6 (Fig. 2.f):** The source vehicle cruising at the center of the 1^{st} lane, communicates with a destination vehicle cruising at the center of the 4^{th} lane, effectively resulting in a lateral shift of $d_h = 3w_l$.

In Scenarios 7 and 8, we consider T-shaped intersections.

- **Scenario 7 (Fig. 2.g):** In this scenario, the source and the destination vehicles are separated from each other with a longitudinal distance of d and there is a horizontal distance of $d_h \approx w_l/2$ between the source vehicle and the intersection point.
- **Scenario 8 (Fig. 2.g):** This scenario is similar to the previous one, but the destination vehicle is closer to the intersection, i.e., $d_h \approx w_l/4$.

In Scenarios 9 and 10, we consider Y-shaped intersections with an intersection angle of $\theta = \arcsin(2w_l/w_s)$ [41] where w_s denotes the intersection width.

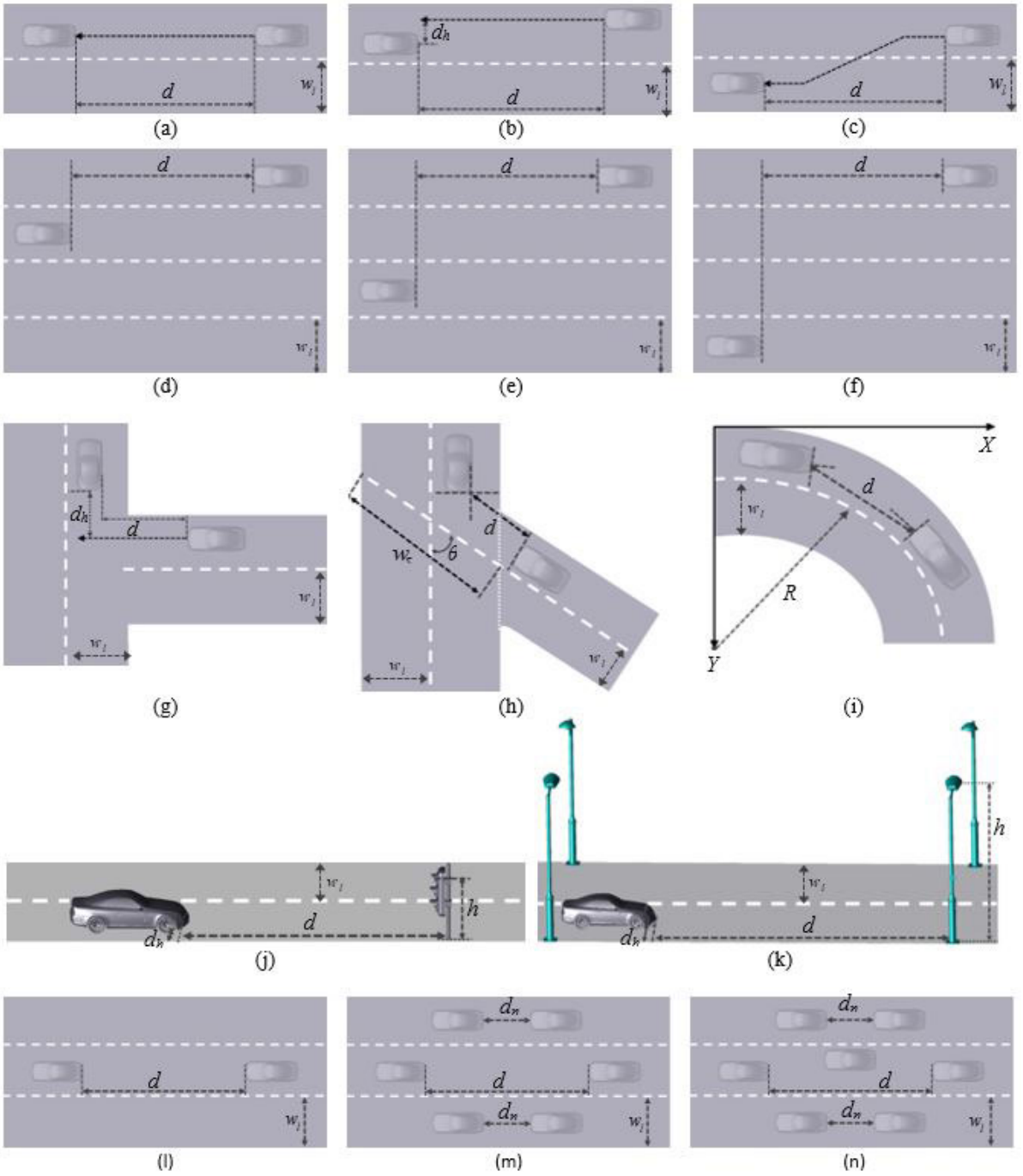

FIGURE 2. Vehicular VLC scenarios under investigation.

- **Scenario 9 (Fig. 2.h):** In this scenario, the source and destination vehicles are separated with a longitudinal distance of d in a T-shaped intersection with a large intersection width, i.e., $w_s \gg 2w_l$.
- **Scenario 10 (Fig. 2.h):** This scenario is similar to the previous one but with relatively smaller intersection width, i.e., $w_s > 2w_l$.

In Scenarios 11 and 12, we consider a curved road with a radius of R where the vehicles are separated from each other with a distance of d.

- **Scenario 11 (Fig. 2.i):** In this scenario, we assume a large road radius, i.e., $R \gg w_l^3$.
- **Scenario 12 (Fig. 2.i):** In this scenario, we assume a relatively smaller road radius, i.e., $R \leq w_l^3$.

In Scenarios 13-15 (Fig. 2.j), we consider I2V link where the traffic light serves as the transmitter which has a height of h. The vehicle is assumed to be at a longitudinal distance of d with respect to the transmitter.

- **Scenario 13:** The vehicle moves at the outer side of the road lane, i.e., $d_h \ll w_l$.

TABLE 3. Vehicular scenarios under consideration.

Scenario	Road Design	Transmitter	Description
Scenario 1	Two-lane Straight road	HLs & TLs	The vehicles follow each other in same lane and with a perfect alignment, i.e., $d_h = 0$.
Scenario 2	Two-lane Straight road	HLs & TLs	The vehicles follow each other in the same lane but there is a misalignment between the vehicles. The maximum lateral shift is considered, i.e., $d_h = w_l - w_v$.
Scenario 3	Two-lane Straight road	HLs & TLs	The two vehicles are moving in the neighbor lanes and the source vehicle changes its lane approaching from the destination one on the target lane.
Scenario 4	Multi-lane Straight road	HLs & TLs	The source vehicle, located at the center of 1^{st} lane, communicates with a destination one that travels at the center of the 2^{nd} lane, i.e., $d_h = w_l$.
Scenario 5	Multi-lane Straight road	HLs & TLs	The source vehicle, located at the center of the 1^{st} lane, communicates with the destination one that travels at the center of the 3^{rd} lane, i.e., $d_h = 2w_l$.
Scenario 6	Multi-lane Straight road	HLs & TLs	The source vehicle, located at the center of 1^{st} lane, communicates with the destination one that travels at the center of the 4^{th} lane, i.e., $d_h = 3w_l$.
Scenario 7	T-Intersection	HLs & TLs	T-shaped road is considered where a distance of $d_h \approx w_l/2$ between the destination vehicle and the intersection point is considered.
Scenario 8	T-Intersection	HLs & TLs	Similar to scenario 4 but with shorter d_h value, i.e., $d_h \approx w_l/4$.
Scenario 9	Y-Intersection	HLs & TLs	Y-shaped road with intersection angle of $\theta = \sin^{-1}(2w_l/w_s)$ and $w_s \gg 2w_l$ is considered.
Scenario 10	Y-Intersection	HLs & TLs	Similar to scenario 6 but with a larger intersection angle, i.e., $w_s > 2w_l$ is assumed.
Scenario 11	Curved-Road	HLs & TLs	Curved road with a large road radius with respect to its width, i.e., $R \gg w_l^3$.
Scenario 12	Curved-Road	HLs & TLs	Similar to scenario 8 but with a shorter road radius, i.e., $R \leq w_l^3$.
Scenario 13	Straight road	Traffic light	The vehicle moves at the outer side of the road lane, i.e., d_h is negligible with respect to w_l.
Scenario 14	Straight road	Traffic light	The vehicle moves at the center of the road lane, i.e., $d_h \approx w_l/4$.
Scenario 15	Straight road	Traffic light	The vehicle moves at the inner side of the road lane, i.e., $d_h \approx w_l/2$.
Scenario 16	Straight road	Streetlights	The vehicle moves at the outer side of the road lane, i.e., d_h is negligible with respect to w_l.
Scenario 17	Straight road	Streetlights	The vehicle moves at the center of the road lane, i.e., $d_h \approx w_l/4$.
Scenario 18	Straight road	Streetlights	The vehicle moves at the inner side of the road lane, i.e., $d_h \approx w_l/2$.

- **Scenario 14:** The vehicle moves at the center of the road lane, i.e., d_h is comparable with w_l.
- **Scenario 15:** The vehicle moves at the inner side of the road lane with the maximum allowable lateral shift, i.e. $d_h = w_l - w_v$.

Scenarios 16-18 (Fig. 2.k) are identical to Scenarios 13-15 except the fact that the street light now serves as the transmitter. The vehicle moves between two street lights separated with a spacing of d_S where the vehicle can receive the data from the two poles.

In Scenarios 19-21, we consider a straight road with three lanes each of which has a width of w_l. The source and destination vehicles are in the middle lane and separated from each other with a longitudinal distance of d. There are also neighbor vehicles either in the same or different lanes.

- **Scenario 19 (Fig.2.l):** This is the benchmark scenario where two connected vehicles follow each other in the middle lane of a three-lane road without any neighbor vehicles.
- **Scenario 20 (Fig.2.m):** In this scenario, there are some neighbor vehicles in the other lanes. neighbor vehicles are assumed to travel in the middle of their lanes and are separated from each other with d_n
- **Scenario 21 (Fig.2.n):** In this scenario, there is an additional neighbor vehicle which travels within the same lane and creates partial blocking to transmission between destination and source vehicles.

The number of PDs to be placed over the vehicle is the choice of system designer. It should be decided in such a way that omni-directional coverage should be ensured in various V2V and I2V scenarios while maintaining a reasonable cost. Considering most typical scenarios detailed above, we conjecture that 9 PDs would be enough to provide a quasi-omni-directional coverage. The locations of PDs are depicted in Fig. 3 and described as follows:

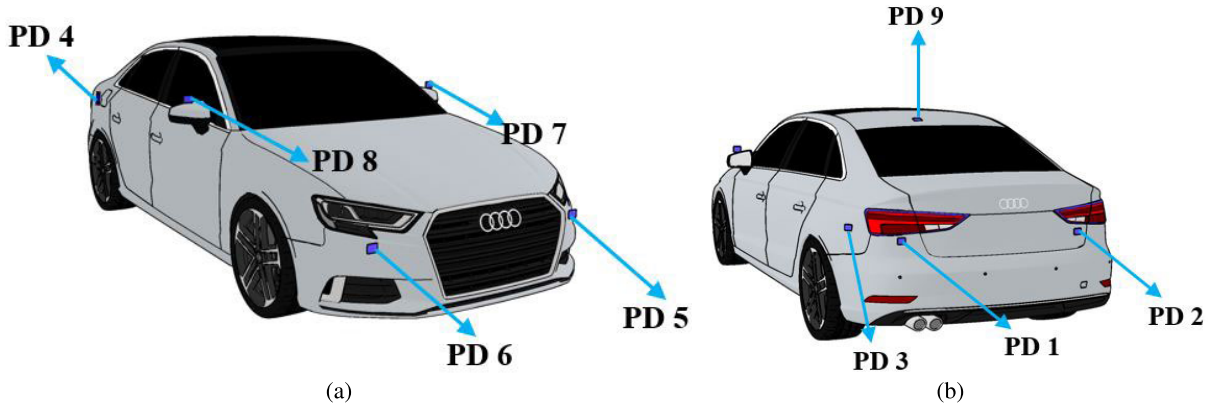

FIGURE 3. Location of photodetectors on the destination vehicle a) Car front view b) Car back view.

- **At the back of the vehicle:** Two PDs (denoted as PD 1 and PD 2) are installed under the TLs. It is expected that they will be primarily useful to receive signals from HLs.
- **At the sides of the vehicle:** Two PDs (denoted as PD 3 and PD 4) are installed at the side-back of the vehicle and at the same height of PD 1 and PD 2. It is expected that PD 3 and PD 4 will be primarily useful when source and destination vehicles are in different lanes or in a curved road.
- **At the front of the vehicle:** Two PDs (PD 5 and PD 6) are installed under the HLs. They are positioned to receive signals from TLs of the front vehicle.
- **At the mirrors:** Two PDs (PD 7 and PD 8) are installed above the mirrors. They are expected to enable I2V links with traffic light transmitters. They might be also useful for V2V links in multi-lane or curved roads.
- **At the top of the vehicle:** A single PD (PD 9) is installed at the top of the vehicle. This is particularly useful for I2V links with street light transmitters.

III. CHANNEL MODELING METHODOLOGY AND PERFORMANCE METRIC

In this section, we first explain our methodology for channel modeling. Then, we define a performance metric to describe the outage which will be later used to interpret simulation results.

A. CHANNEL MODELING METHODOLOGY

Our channel modeling methodology is based on the non-sequential ray tracing features of OpticStudio®. This approach was firstly deployed to model the indoor VLC channels [42]–[44] and experimentally validated in [45], [46]. More recently, it was utilized to model vehicular VLC channels [19], [38], [47]. This approach allows the evaluation of the impulse responses of VLC scenarios with complex geometries and realistic light sources. Radiation pattern of a light source can be defined in the simulation platform by importing its photometric data which contains the luminous intensity in all different planes. It further allows to consider large number of reflections and wavelength-dependent reflectance of the surface material for an accurate modeling. Different types of reflections (specular, diffuse or mixed) can be taken into account by defining the scatter fraction value in the software.

The main steps of this channel modeling methodology are illustrated in Fig. 4. The 3D CAD models for vehicles, roads, and infrastructure poles are designed and imported to the OpticStudio®. The specifications of these CAD models such as coating material, reflectance, and type of reflections are defined. The specifications of the light sources (orientation, radiation pattern, emitted power, etc.) and of the PD (orientation, field-of-view angle, sensitive area, etc.) are provided as other inputs. After the simulation scenario is constructed, non-sequential ray tracing is run to generate an output file containing information about the path length and the received power for each ray emitted from the light source and captured by the detector. Finally, this information is imported into MATLAB®in order to construct the channel impulse response (CIR) for each particular scenario.

B. PERFORMANCE METRIC

Consider the i^{th} transmitter and the j^{th} receiver. Let P_{ij}^{l} and τ_{ij}^{l} denote the optical power and the propagation delay of the l^{th} ray transmitted from the i^{th} LED and received by the j^{th} PD, respectively, $l = 1, \ldots, L_{ij}$. The normalized CIR for unit transmit power is given by [19], [23]

$$h_{i,j}(t) = \sum_{l=1}^{L_{i,j}} P_{i,j}^{l}\, \delta\left(t - \tau_{i,j}^{l}\right) \tag{1}$$

where $\delta(t)$ denotes the Dirac delta function. For a given transmit power of $\delta(t)$, the received optical power at the j^{th} PD from the i^{th} transmitter can be then calculated as

$$Pr_{i,j} = 10\log_{10}\left(Pt_i \int_0^{\infty} h_{i,j}(t)\, dt\right) \tag{2}$$

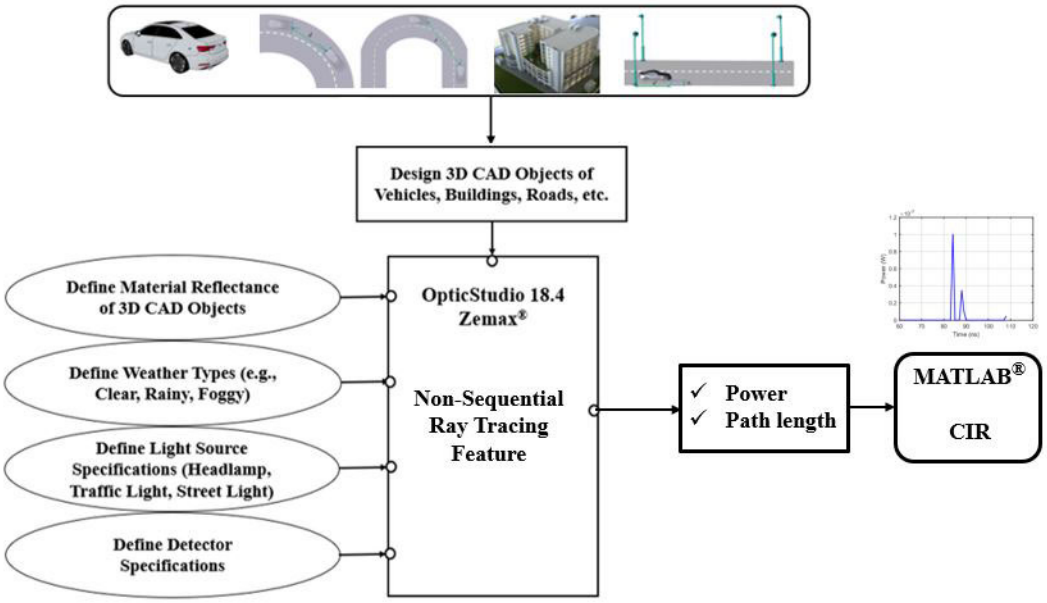

FIGURE 4. Main steps of our channel modeling approach.

The signal-to-noise ratio (SNR) is obtained as

$$\gamma = \frac{\left(\eta \sum_{j=1}^{N_r} Pr_j\right)^2}{N_0 B} \tag{3}$$

where η is the optical-to-electrical conversion ratio, N_r is the number of PDs, N_0 is the noise power spectral density, and B is the bandwidth. Let BER_{th} denote the targeted BER value. In order to avoid outage, the received SNR of the link should be higher than a threshold SNR value of γ_{th} calculated from BER_{th}. Under the assumption of on-off keying (OOK), the minimum required value of received optical power to avoid outage is obtained by [48]

$$Pr_{req} = \sqrt{\frac{N_0 B}{\eta^2}\left(Q^{-1}\left(BER_{th}\right)\right)^2} \tag{4}$$

IV. SIMULATION RESULTS

In this section, we present simulation results for vehicular scenarios under consideration based on non-sequential ray tracing. In our simulation study, Philips Luxeon Rebel white light LEDs [49] and Osram-TOPLED red light LEDs [50] are used for HLs and TLs, respectively. For street lights and traffic lights, Vestel Ephesus M4S [51] and Osram-OSLON® [50] are utilized, respectively. The radiation patterns for HL, TL, traffic light, and street light are presented in Fig. 5. All simulation parameters are provided in Table 4. We consider two different use cases:

- **Low-speed communication with $B = 10$ kHz:** This is sufficient for most safety applications [18], [52]. From (4), it can be readily calculated that a received power of $Pr_{req} \geq -80$ dB is required to achieve $BER_{th} = 10^{-3}$.
- **High-speed communication with $B = 10$ MHz:** This is required to support higher data rates for infotainment applications such as video streaming [53], [54]. This requires a received power of $Pr_{req} \geq -64.7$ dB.

In the following, we first present the total received power versus distance discussing what type of communications can be supported (Section IV.a). Then, in Section IV.b, we discuss the individual contributions of each PD to the total received power and highlight the main use case of each PD.

A. TOTAL RECEIVED POWER VERSUS DISTANCE

In Fig. 6, we present the received power versus distance for Scenarios 1-3 based on either HL transmitters (Fig. 6.a) or TL transmitters (Fig. 6.b). As expected, the received power takes its maximum value when two cars are in perfect alignment (i.e., Scenario 1). In Scenario 2, we assume that there is a misalignment of $d_h = 2$ m between the two vehicles. This misalignment is particularly effective at shorter longitudinal distances. For example, the received power for perfect alignment is -30.8 dB at $d = 10$ m under the assumption of HL transmitters (see Fig. 6.a). This reduces to -32.75 dB in the presence of misalignment. In Scenario 3, it is observed that the rate of change in the received power during the lane changing range (from 15 m to 30 m) is much higher than that in trailing period (from 30 m to 50 m). This is due to that during the lane switching, there is a change in both inter-vehicle distance (d) and lateral shift one (d_h). From Fig. 6, it can be concluded that the received power is sufficient (i.e., $Pr > -45$ dB) for both low- and high-speed communications in these three scenarios when HL transmitters are used to communicate with the preceding vehicle. On the other hand, with the use of TL transmitters, the received

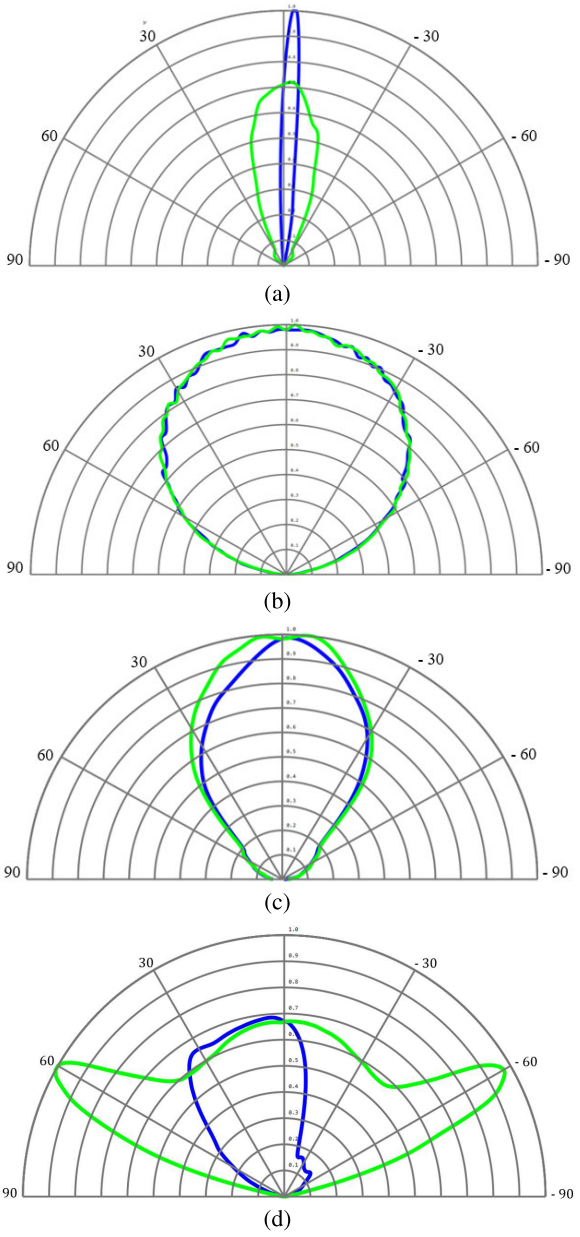

FIGURE 5. Radiation pattern of vehicular light sources in E-plan and H-plane. (a) Headlight (b) Taillight (c) Traffic light (d) Streetlight. For example, in (a), Blue line shows the intensity distribution of headlamp when one looks from side (e.g., from pavement) while the green line shows the pattern when one looks downward from top.

power (i.e., $Pr > -73$ dB) is sufficient only for low-speed communication.

In Fig. 7, we present the received power versus distance for Scenarios 4-6 based on either HL transmitters (Fig. 7.a) or TL transmitters (Fig. 7.b). It is observed that despite the relatively large horizontal displacements, two vehicles in different lanes can successfully communicate with each other. For example, the received power for Scenario 4 (i.e., source and destination vehicles are in neighbor lanes) is -40.9 dB at $d = 25$ m with HL transmitters. This reduces to -47.2 dB and -51.7 dB, respectively for Scenario 5 (i.e., source and destination

TABLE 4. Simulation parameters.

Receiver specifications	Area	1 cm^2
	Field-of-view (FoV)	$90°$
	Responsivity (η)	0.84 (A/W)
	Noise density (N_0)	1×10^{-21} (A^2/Hz)
	Bandwidth (B)	10 kHz, 10 MHz
Road specifications	Type	R2
	Material	Asphalt
	Lane width (w_l)	3.75 m
	Road design	Straight, Intersections, Curved
Vehicle specifications	Length	4.7 m
	Width (w_v)	1.8 m
	Height	1.4 m
	Material	Black gloss paint
Street light pole specifications	Material	Galvanized steel metal
	Spacing (d_S)	20 m
	Height (h)	7 m
Traffic light pole specifications	Material	Galvanized steel metal
	Height (h)	2 m

vehicles are separated from each other with a lane), and Scenario 6 (i.e., source and destination vehicles are separated from each other with two lanes). It can be readily checked that both low- and high-speed communications can be supported when the HLs act as the transmitters. On the other hand, with TL transmitters, the received power is $Pr > -79.87$ dB and therefore satisfies the minimum level to support low-speed communication.

In Fig. 8, we present the received powers versus distance for Scenarios 7-10 where T- and Y-shaped intersections are considered. For T- shaped intersections (Scenarios 7 and 8), it is observed that the value of d_h (the distance between the destination vehicle and the intersection point) has a significant impact on the received power. For example, assuming $d = 25$ m and HL transmitters, the received power for $d_h = 1$ m is -42.7 dB. This reduces to -49.2 dB for $d_h = 2$ m. For Y-shaped intersections (Scenarios 9 and 10), an exponential decay in the received power with d is observed. It is also observed that the intersection angle θ has a little effect on the received power. For example, the received power for $\theta = 45°$

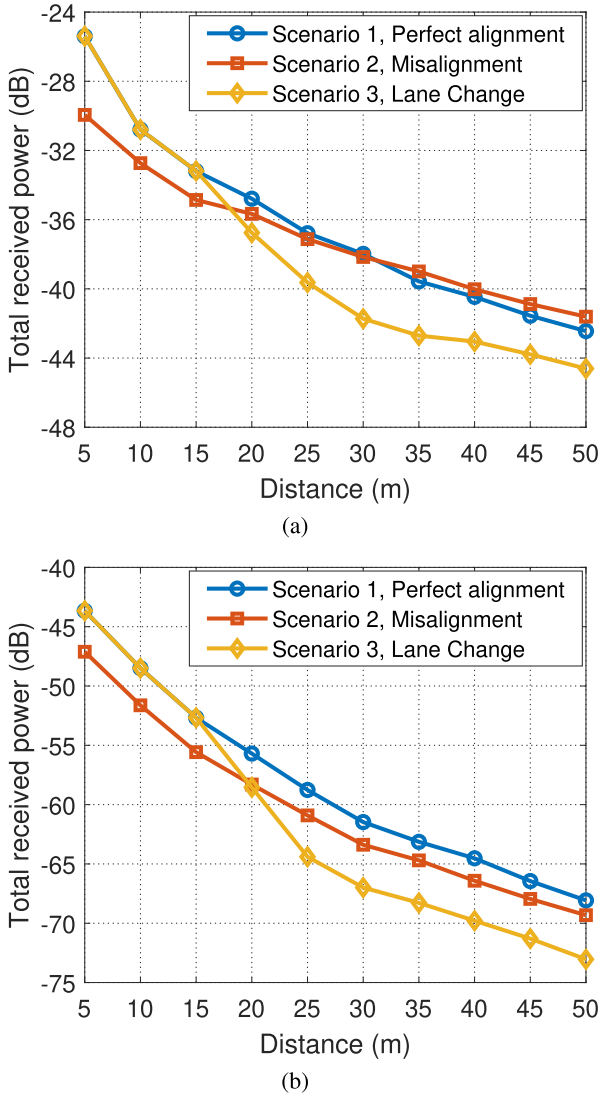

FIGURE 6. Total received power for V2V in straight road scenarios based on (a) HLs (b) TLs.

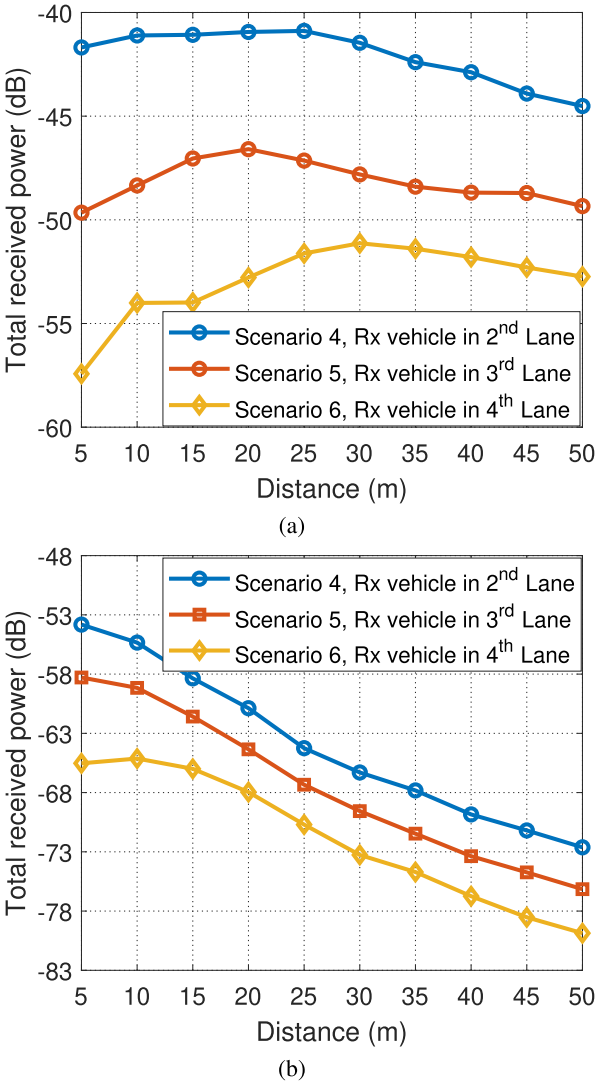

FIGURE 7. Total received power for V2V in multi-lanes scenarios based on (a) HLs (b) TLs.

is -64.4 dB assuming TL transmitters and $d = 30$ m. This slightly reduces to -64.75 dB for $\theta = 60°$. From Fig. 8, it can be concluded that the received power is sufficient (i.e., $Pr > -51.5$ dB) for both low- and high-speed communications in these four scenarios with HL transmitters. Based on the use of TL transmitters, the received power is sufficient (i.e., $Pr > -81.5$ dB) only for low-speed communication.

In Fig. 9, we present the received power versus distance for Scenarios 11-12 where a curved road is considered. It is observed that the received power significantly reduces when the road radius (R) decreases. For example, consider $d = 40$ m and HL transmitters. As observed from Fig. 9.a, the received powers for $R = 100$ m and $R = 50$ m are respectively -55.5 dB and -69.6 dB. It can be also observed that the received power much depends on the curve radius same as the propagation distance. At shorter radius together with larger distance, the received power is much reduced, and the system outage might occur particularly take place when high data rate is targeted. It can be readily checked that the received power in Scenario 11 is sufficient (i.e., $Pr > -61.9$ dB) for both low- and high-speed communications with HL transmitters while the received power in Scenario 12 remains lower than the minimum level of -64.7 dB. Based on the use of TL transmitters, the received power in these scenarios is sufficient (i.e., $Pr > -79$ dB) only for low-speed communication.

In Fig. 10, we present the received power versus distance for I2V scenarios based on either traffic light transmitters (Scenarios 13-15, Fig. 10.a) or street light transmitters (Scenarios 16-18, Fig. 10.b). It is observed from Fig. 10.a that the received power is affected by the particular position of the vehicle with respect to traffic light transmitter. As observed from Fig. 10.a, the received power at $d = 10$ m for $d_h = 0$ m (i.e., the vehicle is located at the outer side of the road lane) is -43.6 dB. This reduces to -44.55 dB and -45.53 dB for $d_h = 1$ m and $d_h = 2$ m, respectively.

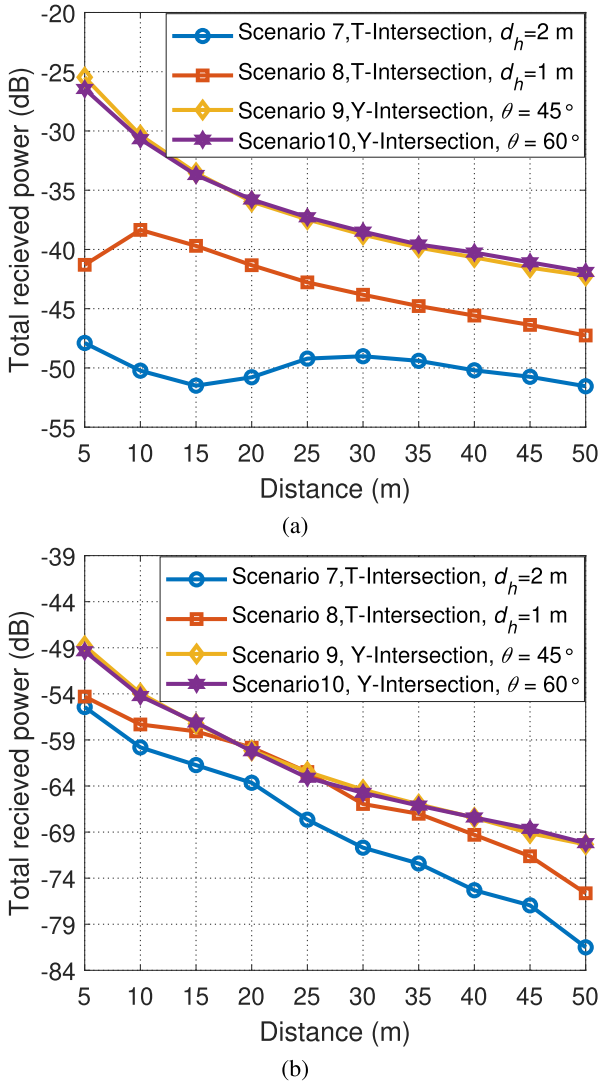

FIGURE 8. Total received power for V2V in intersection scenarios based on (a) HLs (b) TLs.

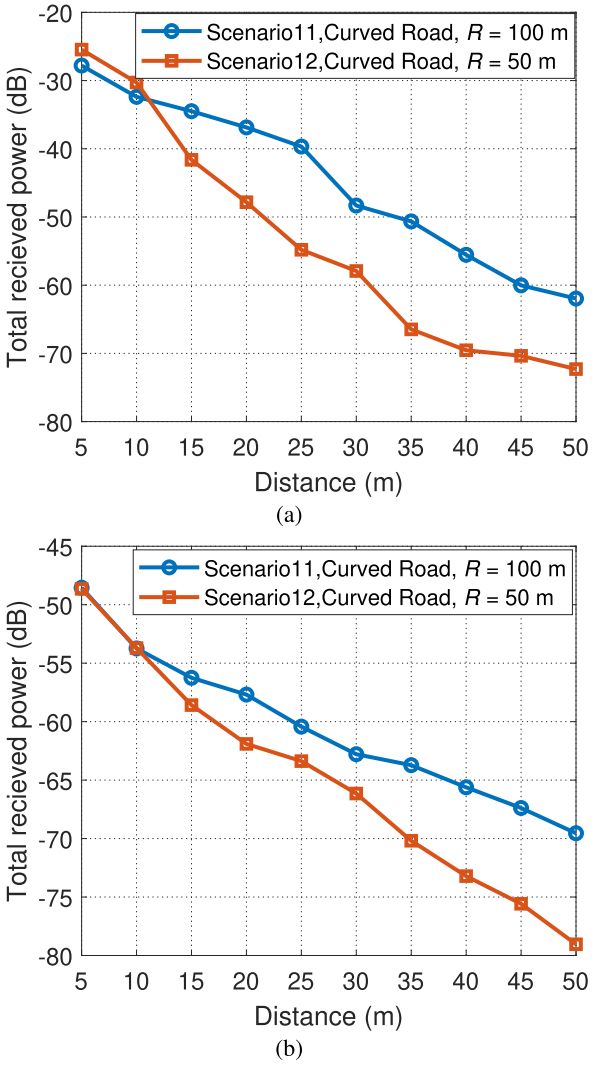

FIGURE 9. Total received power for V2V in curved road scenarios based on (a) HLs (b) TLs.

In Fig. 10.b, the street lights serve as transmitters where the vehicle moves between two street light poles separated with $d_S = 20$ m. Under the first pole, only PD 9 (located on the top of the vehicle) can collect a significant amount of the power. This is due to the fact that PDs 5-8 cannot see this transmitter, and PDs 1-4 (which are looking to the second pole) are still far. When the vehicle moves away from the first pole, the received power decreases. If the distance becomes sufficiently large ($d > 4$ m), the PDs 5-8 are now able to collect power. In particular PD 7 and 8 (located on the top of the mirrors) along with PD9 collect most of the power. When the vehicle approaches the second pole, the contributions of PDs 5-8 relatively decrease while there is some increase in received powers of PDs 1-4. In particular, PD 4 (located at same side of closer street lights) reaches its maximum value at $d = 16$ m. After that, it reduces to reach its minimum value when the vehicle arrives under the second pole ($d = 20$ m). At this point, a significant power is only collected again by PD 9. It can be readily checked that for all I2V scenarios under consideration, the received power is much higher than the required power to support both low- and high-speed communications.

In Fig. 11, we present the received power versus distance for Scenarios 19-21 where the effect of neighbor vehicles and partial blockage are considered. In Scenario 20, it is observed that the received power slightly increases in comparison to the benchmark scenario (i.e., Scenario 19) as a result of receiving additional amount of power reflected from the neighbor vehicles. This is observed only at sufficiently large distances ($d \geq 40$ m). The reason for that is at larger distances, the reflecting surface at the two sides of neighbor vehicles increases and hence the number of reflected rays reaching the PD increases. At shorter distances, the amount of received power from such reflections is negligible. In Scenario 21, a significant reduction in the received power is observed in

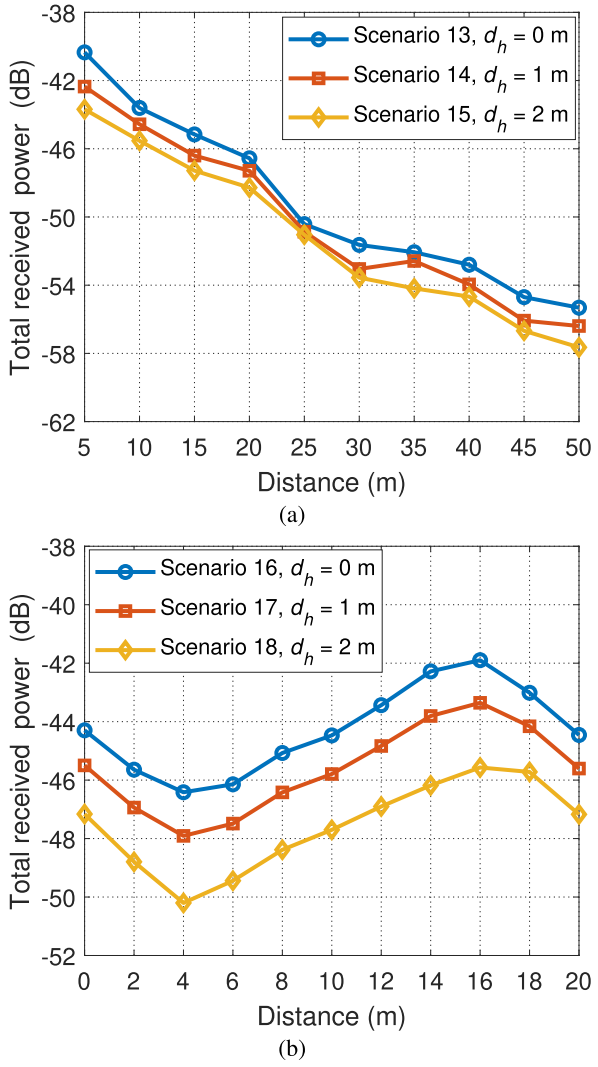

FIGURE 10. Total received power for I2V scenarios based on (a) Traffic lights (b) Streetlights.

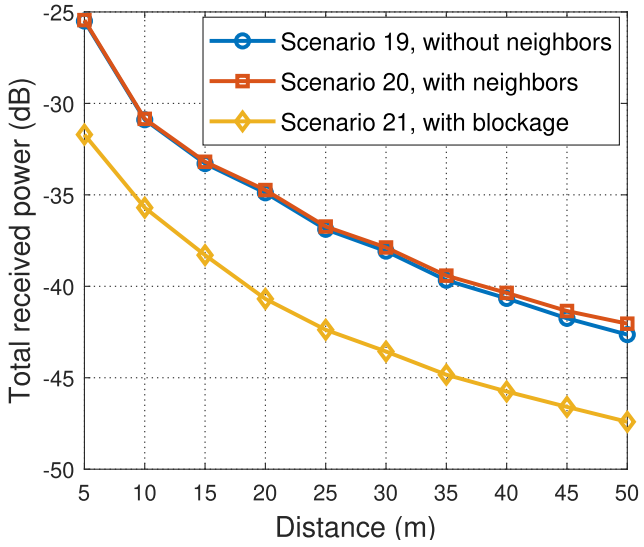

FIGURE 11. Total received power for V2V scenarios with neighboring vehicles.

comparison with Scenarios 19 and 20. This is due to the effect of partial blockage by the neighbor vehicle which travels in the same lane. For example, consider $d = 50$ m. The received power for scenario 19 is -42.6 dB. This increases to -42 dB and reduces to -47.4 dB for scenario 20 and 21, respectively. From Fig. 11, it can be further concluded that the received power is sufficient (i.e., $Pr > -47.5$ dB) for both low- and high-speed communications.

B. CONTRIBUTIONS OF EACH PD AND DISCUSSIONS ON USE CASES

In the previous section, we presented the total power versus distance for different scenarios under consideration. In this section, we quantify which PDs contribute at what extent to total received power.

In Fig. 12.a, we present pie charts for Scenarios 1, 2 and 3 based on HL transmitters.

- In Scenario 1 where two cars are perfectly aligned, the deployment of only two photodetectors in the back (i.e., PD 1 and PD 2) would be sufficient. These two PDs collect 98% or more of the total power based on the distance. For large distances, PD 3 and PD 4 collect a small amount as a result of road reflections if the distance between two vehicles is sufficiently large, e.g., about 2% at a distance of $d = 50$ m.
- In Scenario 2 when there is some displacement (towards the left-hand side) between two vehicles, it is observed that PD 1 and PD 3 (located on left-hand side of the destination vehicle) are primary receptors. The contribution of PD 2 increases with the increase in distance since the effect of lateral displacement becomes negligible for large distances. It should be noted that if the displacement is towards the right-hand side, PD 2 and PD 4 would be primary receptors.
- In Scenario 3, the lane change occurs from the left-hand side to the right-hand side. It is observed that within initialization range (from 10 m to 15 m), PD 1 and PD 2 can collect almost all power (i.e., 100%) due to the proper alignment between the two vehicles. However, during the lane change range (from 15 m to 30 m) and trailing range (from 30 m to 50 m), PD 3 collects the highest amount of received power (i.e., 40%) while the contributions of PD 1 and PD 2 are reduced.

In Fig. 12.b, we present pie charts for Scenarios 1, 2 and 3 based on TL transmitters.

- In Scenario 1 where two cars are perfectly aligned, PD 5 and PD 6 capture most of the received power if the distance is sufficiently small. When distance gets larger, the contributions of PD 7 and PD 8 are more pronounced since the height difference between the TL transmitters and PD 7 / PD 8 gets smaller.

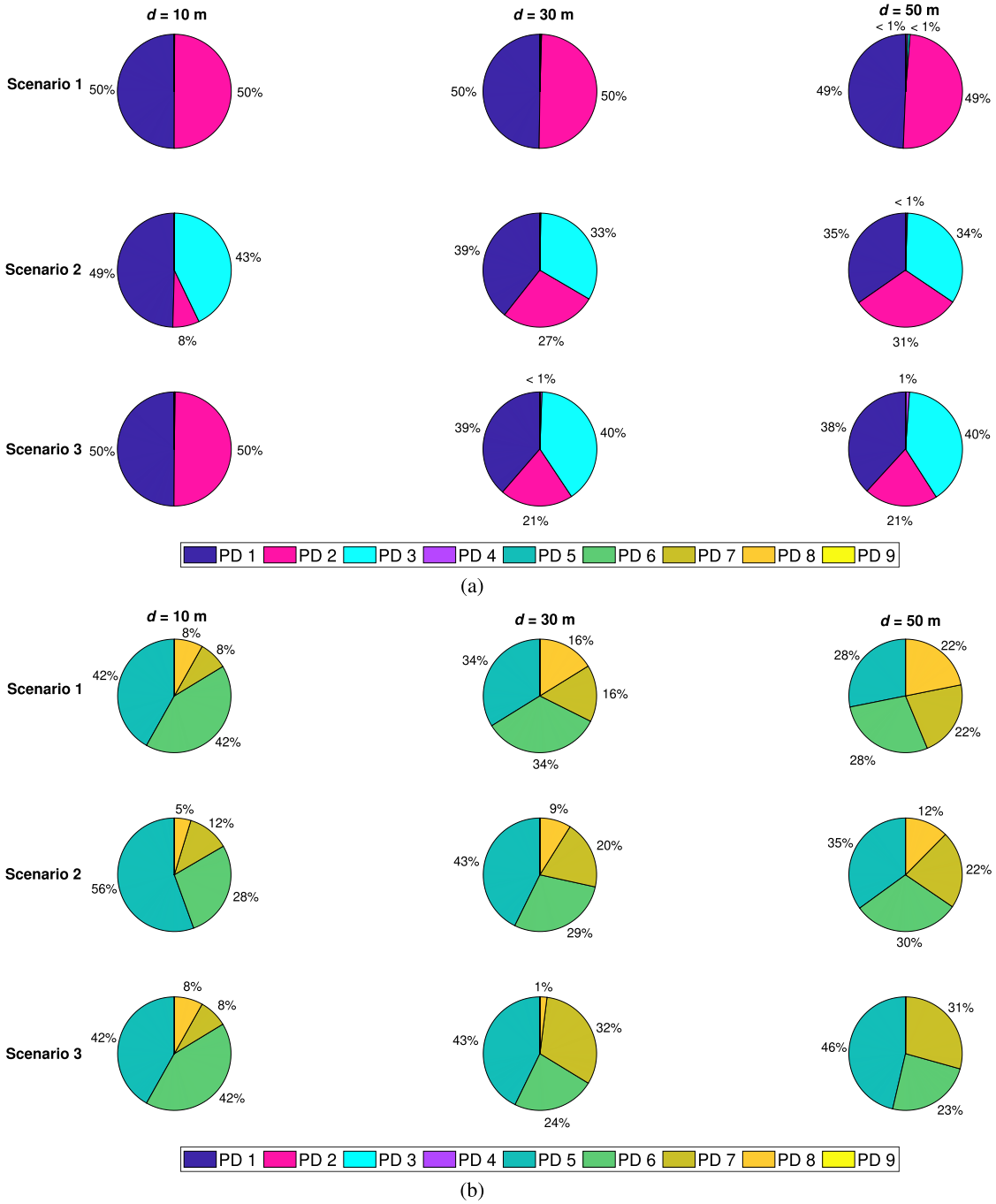

FIGURE 12. **Contribution of each PD for V2V in straight road scenarios based on (a) HLs (b) TLs.**

- In Scenario 2 when there is some displacement (towards the left-hand side) between two vehicles, PD 5 and PD 6 remain as the primary receptors. However, in comparison to Scenario 1, the contribution of PD 6 is now reduced since it is located on the other side of the displacement.
- In Scenario 3, PD 5 and PD 6 collect most of the power within the initialization range (from 10 m to 15 m) while a small amount of received power is collected with PD 7 and PD 8. During the lane change range (from 15 m to 30 m) and trailing range (from 30 m to 50 m), PD 5, PD 6 and PD 7 collect almost all power and the contribution of PD 8 becomes negligible.

In Fig. 13.a, we present pie charts for Scenarios 4, 5, and 6 based on HL transmitters.

- In these three scenarios, PD1 and PD 3 (located on the same side of the source vehicle) are the primary receptors. PD2 also contributes to the received power to some

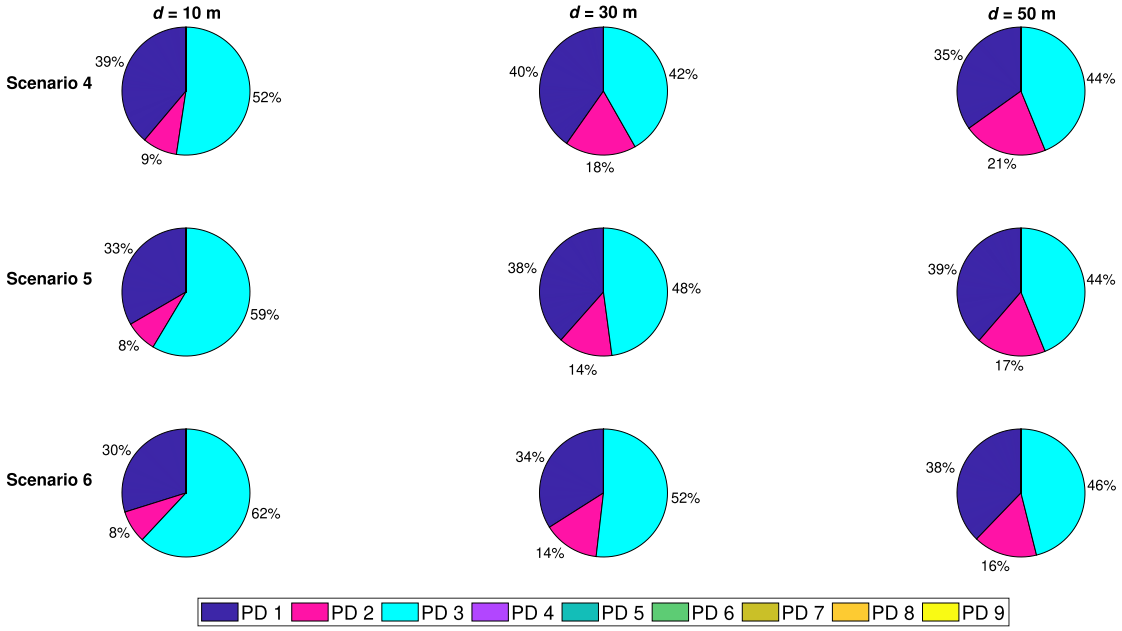

(a)

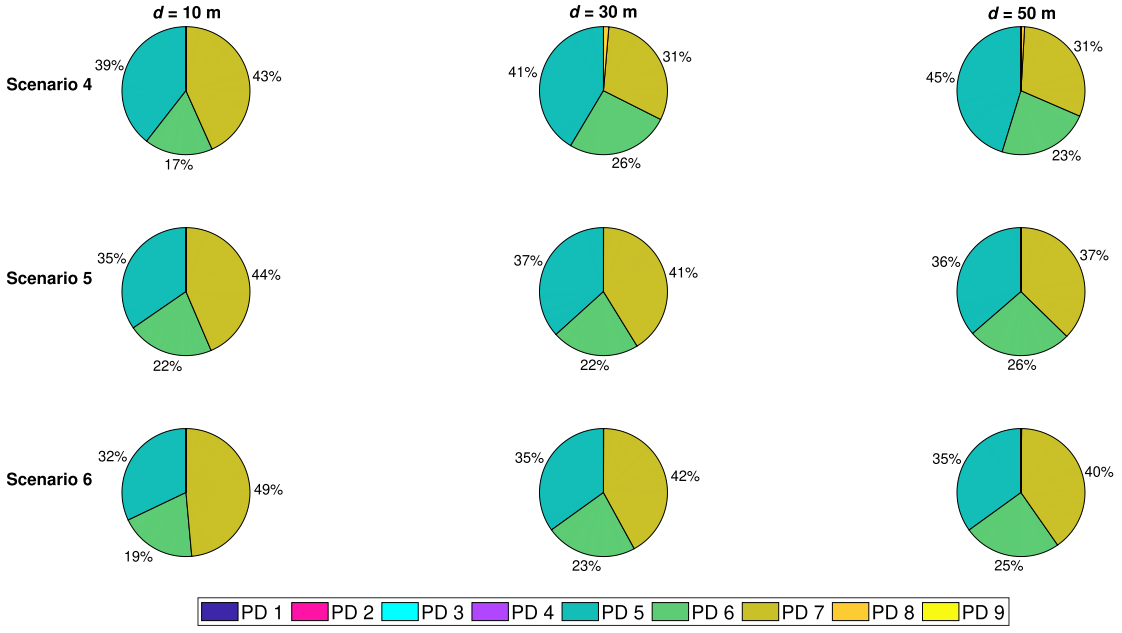

(b)

FIGURE 13. Contribution of each PD for V2V in multi-lane scenarios based on (a) HLs (b) TLs.

extent. With the increase in distance, the contribution of PD 2 increases. Because at sufficiently large distances, PD 2 is able to see both HLs of the source vehicle.

In Fig.13.b, we present pie charts for Scenarios 4, 5, and 6 based on TL transmitters.

- In these three scenarios, PD5 and PD 7 (located on the same side of the source vehicle) are the primary receptors. PD 6 comes as the third largest contributor to the received power. Its contribution particularly becomes large for large distances. Finally, only a very small received power is collected by PD 8 as a result of road reflections if the distance between two vehicles is sufficiently large.

In Fig. 14.a, we present pie charts for Scenarios 7, 8, 9, and 10 based on HL transmitters.

- In Scenarios 7 and 8 where T-shaped intersection is considered, PD 3 collects most of the received power (e.g.,73% or more) due to its location on the side of

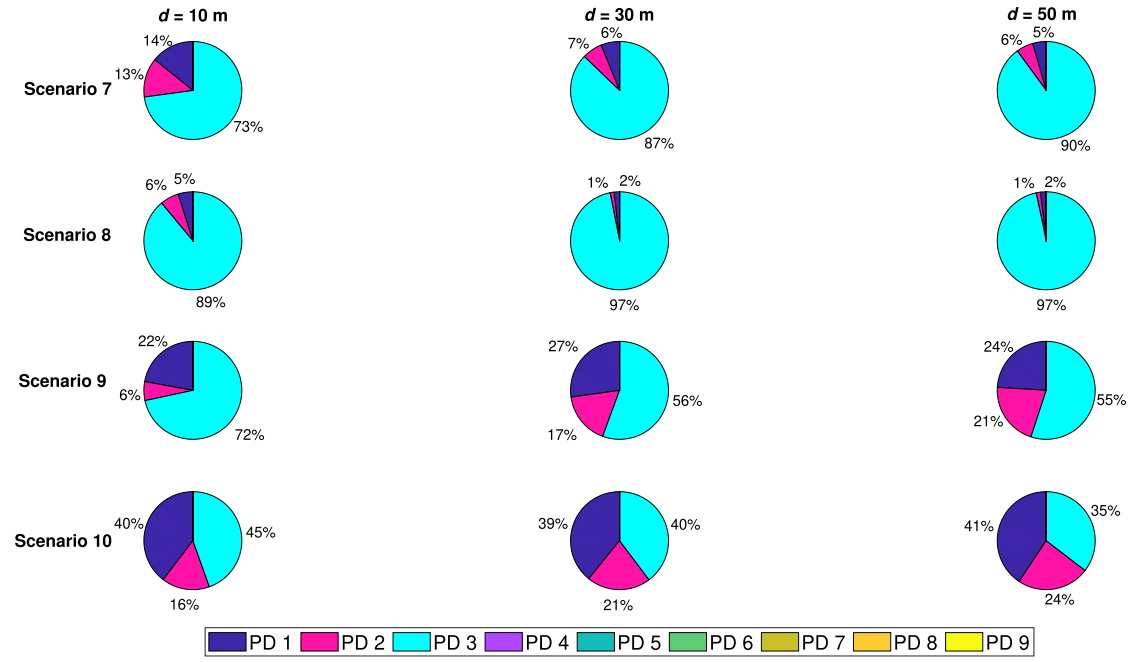

(a)

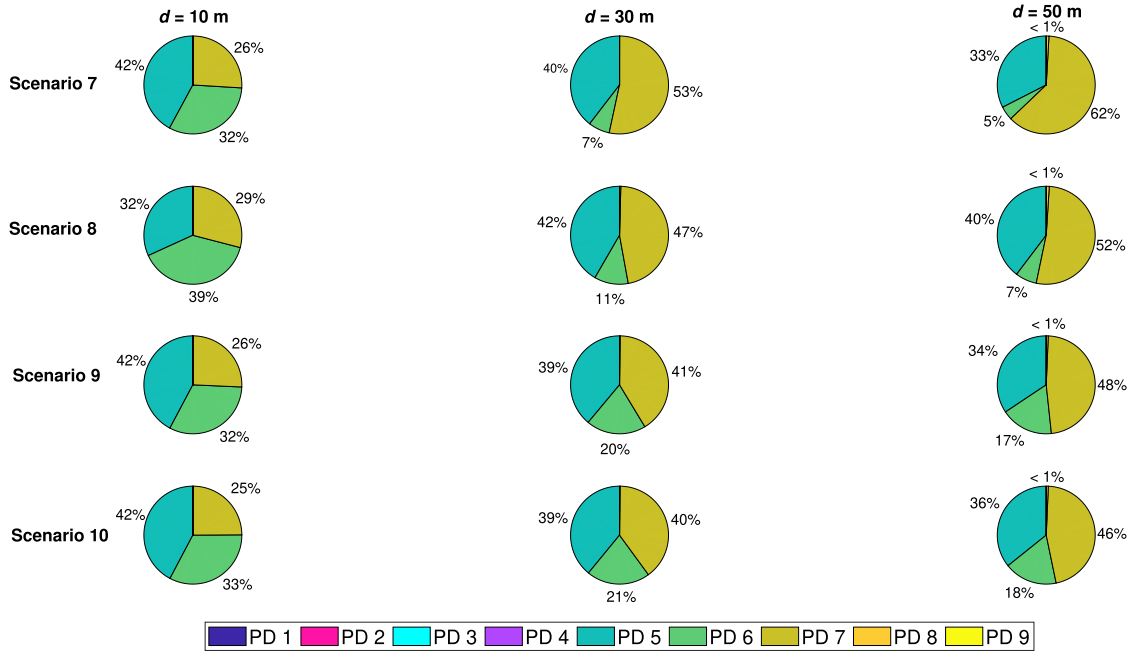

(b)

FIGURE 14. **Contribution of each PD for V2V in intersection road scenarios based on (a) HLs (b) TLs.**

intersection point. The rest of received power is collected by PD 1 and PD 2 and their contribution further decreases when either the longitudinal distance (d) or the horizontal one (d_h) increases.

- In Scenarios 9 and 10 where Y-shaped intersection is considered, PD 1 and PD 3 are the main receptors. For Scenario 9 where lower skew angle is considered (i.e., $\theta = 45°$), the contribution of PD 3 is approximately twice of PD 1 if the distance between the vehicles is sufficiently large. In Scenario 10 where a larger skew angle is considered (i.e., $\theta = 60°$), PD 1 is able to collect approximately same power amount of PD 3. In addition, PD 2 collects some power which increases when the distance gets larger.

In Fig. 14.b, we present pie charts for Scenarios 7, 8, 9, and 10 based on TL transmitters.

- In Scenarios 7 and 8 where T-shaped intersection is considered, PD 5 and PD 6 collect the highest amount of received power for shorter longitudinal distances. When the distance between two vehicles increases,

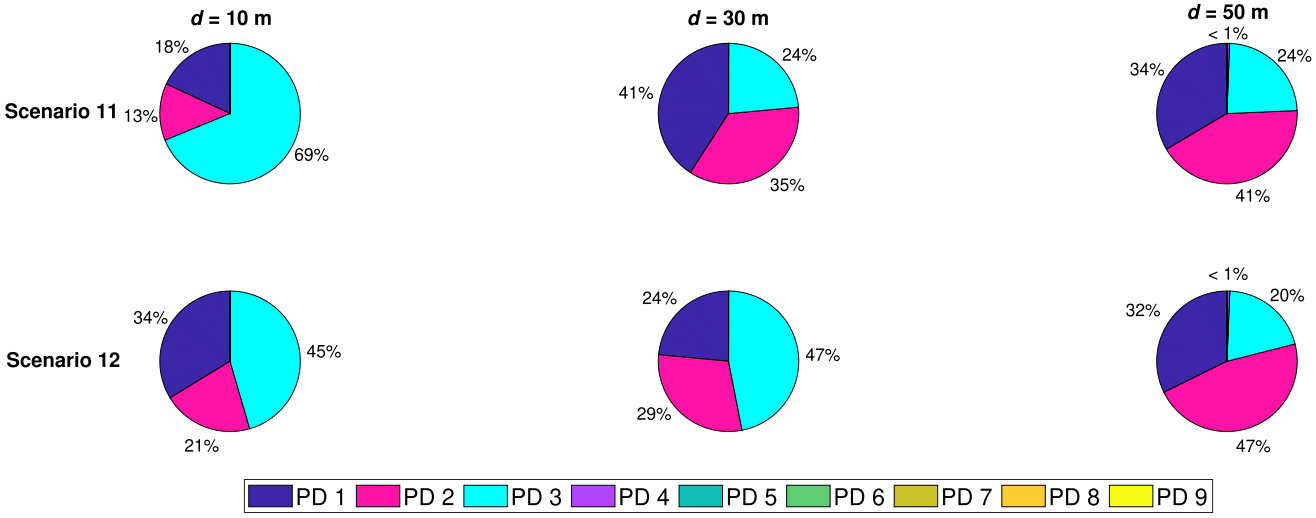

(a)

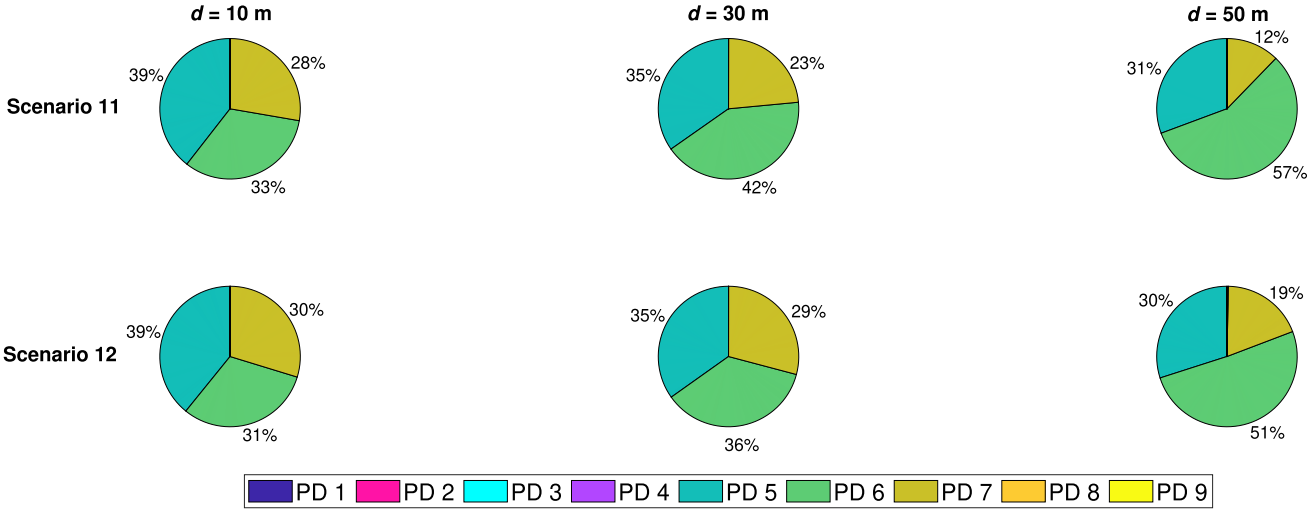

(b)

FIGURE 15. Contribution of each PD for V2V in curved road scenarios based on (a) HLs (b) TLs.

the contribution of PD 7 much increases while the received power using PD 6 is significantly reduced because of its location on the other side of intersection point. A very small portion of received power is collected by PD 8 as a result of road reflections for sufficiently large distances.

- In scenarios 9 and 10 where Y-shaped intersection is considered, PD 5 collects the highest amount of received power for short distances. At larger distances, the contribution of PD 5 decreases while the contribution of PD 7 increases. Particularly at shorter distances, a significant amount of received power is collected by PD 6.

In Fig. 15.a, we present pie charts for Scenarios 11 and 12 based on HL transmitters.

- In Scenarios 11 and 12, curved roads with radii of $R = 100$ m and $R = 50$ m are considered, respectively. At shorter distances PD 3 collects the highest amount of received power (i.e., 69% at $d = 10$ m and Scenario 11) while contributions of PD 1 and PD 2 are somewhat limited. When the distance increases, the received power using PD 1 and PD 2 increases. For sufficiently large distance, the contribution of PD 2 becomes the maximum (41%) followed by PD 1 (34%) and PD 3 (24%). This is due to that with increasing the distance the direction of the source vehicle moves away from PD 3 and towards PD 2. In other words, the angle of arrival at PD 2 is smaller compared to PD 3.

In Fig. 15.b, we present pie charts for Scenarios 11 and 12 based on TL transmitters.

- In Scenarios 11 and 12, it is observed that PD 5 and PD 6 always collect the highest received powers (i.e., 70% or more based on the distance). The contribution of PD7 decreases with increase in distance.

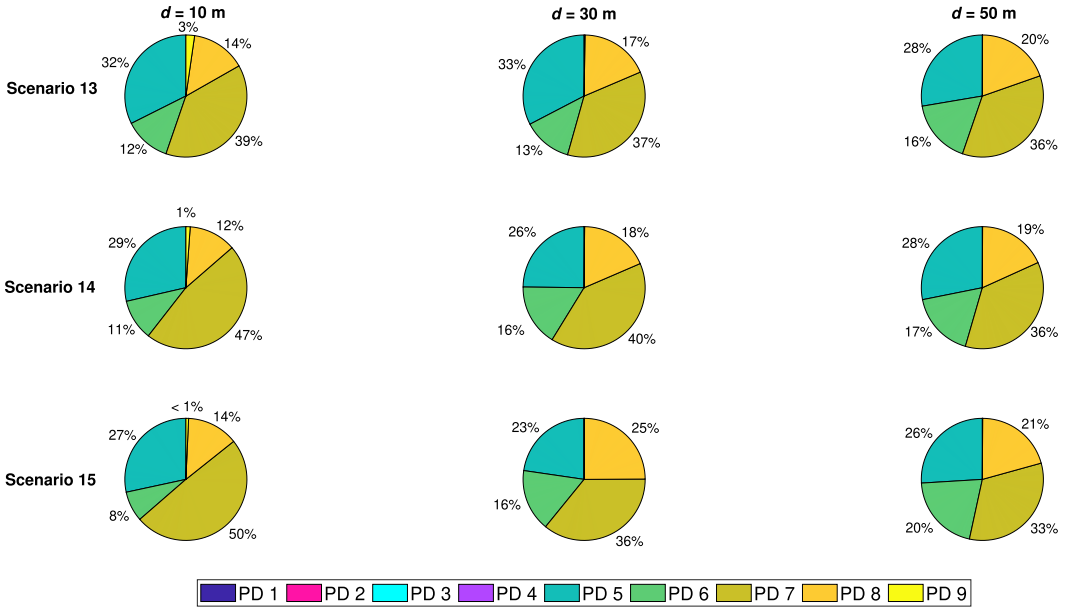

(a)

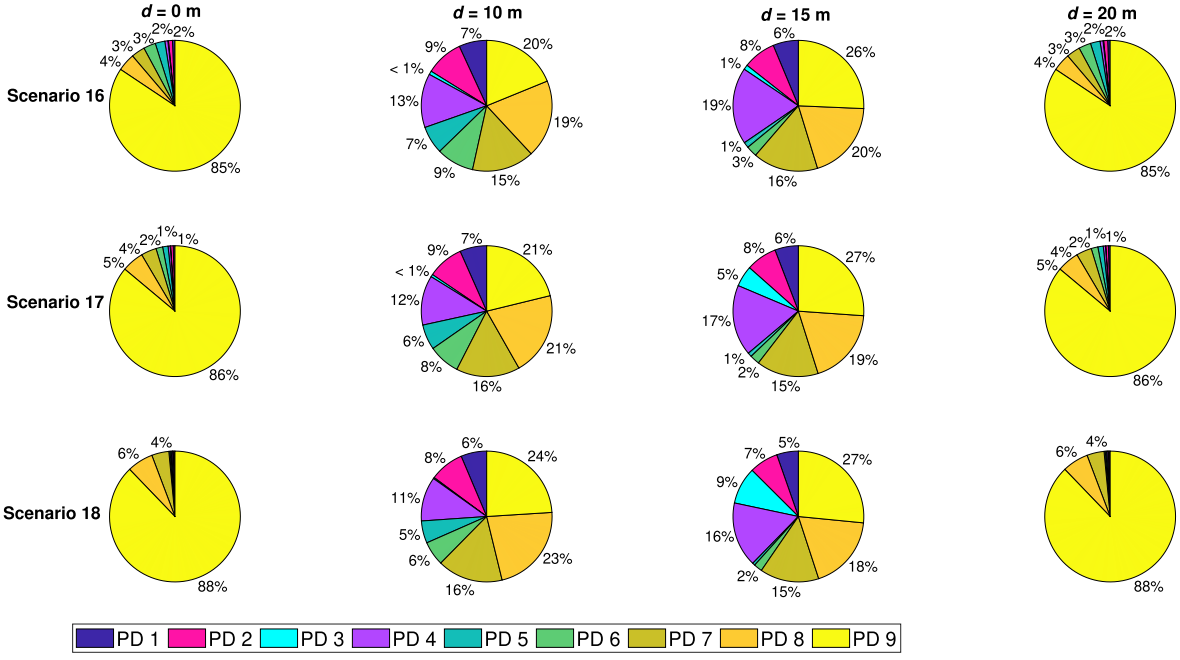

(b)

FIGURE 16. **Contribution of each PD for I2V scenarios based on (a) Traffic lights (b) Streetlights.**

In Fig. 16, we present pie charts for Scenarios 13-15 based on traffic light transmitters and for Scenarios 16-18 based on street light transmitters.

- In Scenarios 13-15 (see Fig. 16.a), the traffic light is the transmitter. It is observed that PD 5 and PD 7, located at the right-hand side, collect the highest amount of received power, i.e., 59% and more. In Scenario 13 ($d_h = 0$ m), a small difference is observed between received powers of PD 5 and PD 7. In Scenarios 14 and 15 where d_h increases respectively to 1 m and 2 m, the difference gets larger particularly at shorter distances. It is further observed that contributions of PD 6 and PD 8 (located at the left-hand side) improve with the increase in distance.
- In Scenarios 16-18 (see Fig. 16.b), the street lights are transmitters. At small distances, PD 9 located at the top of the vehicle is the primary receptor. As distance increases, all 9 PDs contribute at different levels to

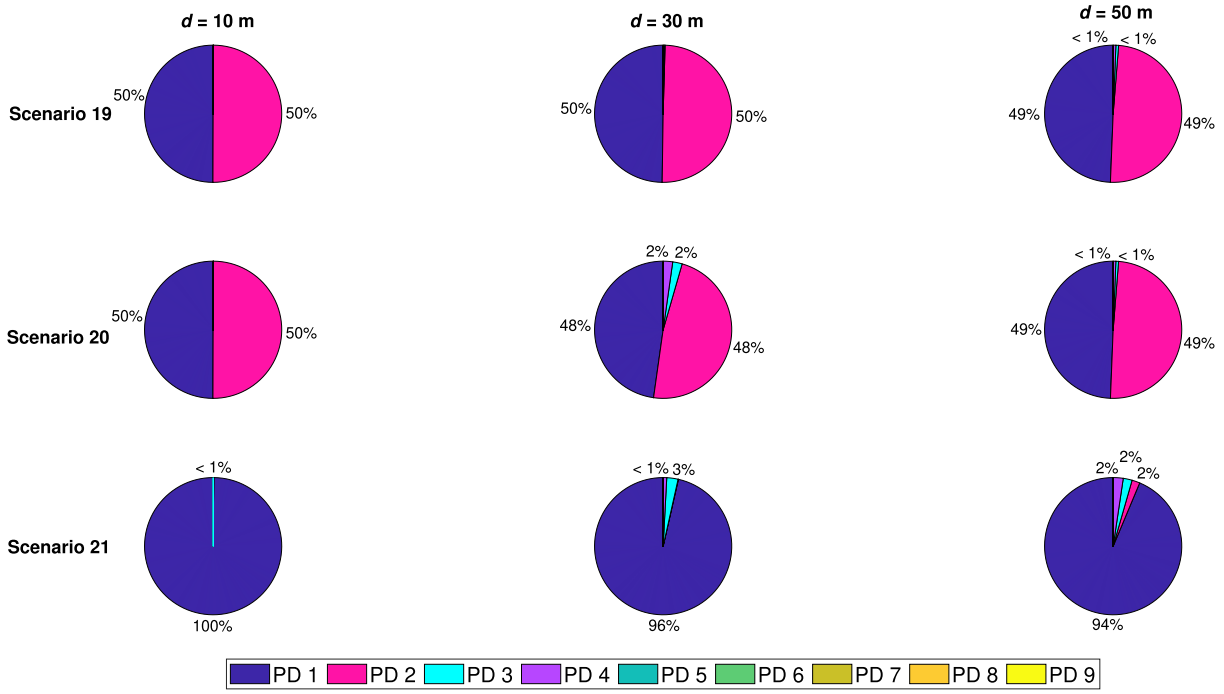

FIGURE 17. Contribution of each PD for V2V scenarios with neighboring vehicles.

the received power although PD 9 always receives the highest received power.

In Fig. 17, we present pie charts for Scenarios 19, 20, and 21.

- In Scenario 19 and 20 where two vehicles follow each other in the middle lane with and without neighbor vehicles (i.e., no blockage), PD 1 and PD 2 are the main receptors. These two PDs collect 96% or more of the total power based on the distance. A small amount of received power is collected using PD 3 and PD 4 because of road reflections if the distance between two vehicles is sufficiently large.
- In Scenario 21 where partial blockage occurs, PD 1 becomes the primary receptor which collects 94% or more of the total power based on the distance. On the other side, the received power using PD 2 becomes negligible (i.e., only 2% due to reflections and at sufficiently larger distances). This is due to its location on the side of blockage vehicle. It should be noted that if the blockage vehicle is re-located at the left-hand side, PD 2 would be primary receptor.

C. EFFECT OF NEIGHBOR VEHICLES ON SINR

It should be emphasized that received power by its own might not be sufficient to evaluate the performance in Scenarios 19, 20, and 21 where there are neighbor vehicles. In particular, we need to impose some assumption on the transmitters of the neighbor vehicles and accordingly calculate signal-to-interference-plus-noise ratio (SINR). In the first case, the neighbor vehicles are assumed to have inactive HLs transmitters. In this case, the HLs are used only for illumination purposes with no signal transmission. The received light from neighbors with inactive transmitters is treated as shot noise in SINR calculation. In the second case where the transmitters are assumed to be active, the received lights from neighbor vehicles are considered as interfering signals in SINR calculation.

In Fig. 18.a, we present the SINR results for the case of inactive transmitters and assume high speed communication, i.e., $B = 10$ MHz. Similar to our earlier observations in Fig.11, the presence of neighbor vehicles in other lanes improves received SINR due to additional reflections. On the other side, when there is a blockage (i.e., Scenario 21) the received SINR is significantly degraded.

In Fig. 18.b, we consider the case of active transmitters and assume $B = 10$ MHz. It is observed in Scenario 20 that the received SINR value significantly reduces (i.e., $\geq$57 dB) with respect to Scenario 19. In Scenario 21, it is observed that the blockage vehicle further reduces the SINR values (i.e., $\leq$6 dB) with respect to Scenario 20. This is due to the fact that the blockage affects both the desired and the interfering signals. Despite the degrading effects of neighbor vehicles, the received power values are sufficient for both low-speed and high-speed communication use cases. In particular, the threshold SINR value required to achieve our target of $\text{BER}_{th} = 10^{-3}$ is given as $\gamma_{th} = 9$ dB.[1] It is observed from Fig. 18 that SINR value of 15.7 dB is achieved at a

[1]For OOK under consideration, the threshold SINR (γ_{th}) required to achieve a target BER of (BER_{th}) is given as $\gamma_{th} = \left(Q^{-1}\left(BER_{th}\right)\right)^2$ [47]. For $\text{BER}_{th} = 3.8 \times 10^{-3}$ (i.e., the 7% forward error correction BER limit [48]), a threshold SNR of $\gamma_{th} = 8.6$ dB is required.

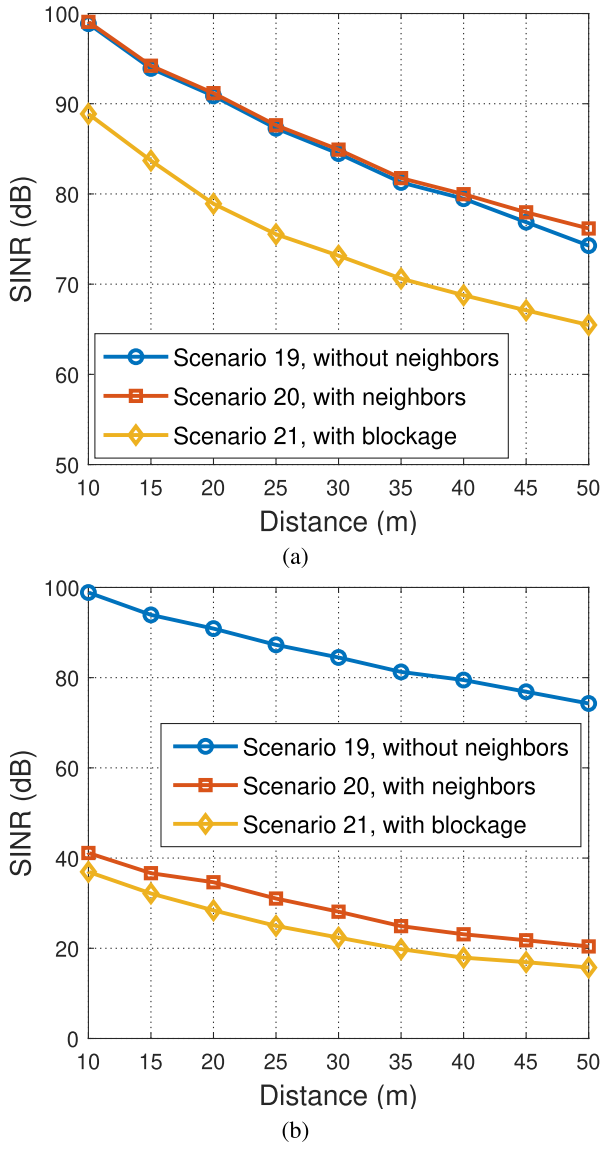

FIGURE 18. Effect of neighboring vehicles and blockage on the received SINR (a) Case A, i.e., inactive transmitters and (b) Case B, i.e., active transmitters.

distance of 50 m even in the case of heavy traffic described by Scenario 21.

V. CONCLUSION

In this paper, we investigated the coverage of a vehicular VLC system in an effort to determine the number and location of PDs. Based on non-sequential ray tracing, we conducted a channel modeling study to determine the received powers for various V2V and I2V scenarios. Our results revealed that deployment of nine PDs with carefully determined locations on the vehicle would be sufficient to support both V2V connectivity (in front and back directions) and I2V connectivity in different road types, intersections, and traffic scenarios. The contribution of each PD was also quantified to indicate which PDs are the primary and optional receptors for each scenario under investigation.

ACKNOWLEDGMENT

The author Hossien B. Eldeeb thanks Dr. Mohamed Elamassie and Eng. Sadi Safaraliev for their help and support. This article was presented in part at IEEE International Conference in Electrical and Electronics Engineering (ELECO'19).

REFERENCES

[1] O. Pribyl, P. Pribyl, M. Lom, and M. Svitek, "Modeling of smart cities based on ITS architecture," *IEEE Intell. Transp. Syst. Mag.*, vol. 11, no. 4, pp. 28–36, Nov. 2019.

[2] R. Miucic, *Connected Vehicles: Intelligent Transportation Systems*. Cham, Switzerland: Springer, 2019.

[3] S. Chen, J. Hu, Y. Shi, Y. Peng, J. Fang, R. Zhao, and L. Zhao, "Vehicle-to-everything (V2X) services supported by LTE-based systems and 5G," *IEEE Commun. Standards Mag.*, vol. 1, no. 2, pp. 70–76, Jun. 2017.

[4] Z. MacHardy, A. Khan, K. Obana, and S. Iwashina, "V2X access technologies: Regulation, research, and remaining challenges," *IEEE Commun. Surveys Tuts.*, vol. 20, no. 3, pp. 1858–1877, 3rd Quart., 2018.

[5] G. Naik, J. Liu, and J.-M. Park, "Coexistence of wireless technologies in the 5 GHz bands: A survey of existing solutions and a roadmap for future research," *IEEE Commun. Surveys Tuts.*, vol. 20, no. 3, pp. 1777–1798, 3rd Quart., 2018.

[6] K. Z. Ghafoor, M. Guizani, L. Kong, H. S. Maghdid, and K. F. Jasim, "Enabling efficient coexistence of DSRC and C-V2X in vehicular networks," *IEEE Wireless Commun.*, vol. 27, no. 2, pp. 134–140, Apr. 2019.

[7] X. Cai, B. Peng, X. Yin, and A. P. Yuste, "Hough-transform-based cluster identification and modeling for V2V channels based on measurements," *IEEE Trans. Veh. Technol.*, vol. 67, no. 5, pp. 3838–3852, May 2017.

[8] M. Uysal, Z. Ghassemlooy, A. Bekkali, A. Kadri, and H. Menouar, "Visible light communication for vehicular networking: Performance study of a V2V system using a measured headlamp beam pattern model," *IEEE Veh. Technol. Mag.*, vol. 10, no. 4, pp. 45–53, Dec. 2015.

[9] A.-M. Cailean and M. Dimian, "Impact of IEEE 802.15.7 standard on visible light communications usage in automotive applications," *IEEE Commun. Mag.*, vol. 55, no. 4, pp. 169–175, Apr. 2017.

[10] B. M. Masini, A. Bazzi, and A. Zanella, "Vehicular visible light networks for urban mobile crowd sensing," *Sensors*, vol. 18, no. 4, p. 1177, 2018.

[11] B. M. Masini, A. Bazzi, and A. Zanella, "Vehicular visible light networks with full duplex communications," in *Proc. 5th IEEE Int. Conf. Models Technol. Intell. Transp. Syst. (MT-ITS)*, Jun. 2017, pp. 98–103.

[12] A. I. Petrariu, A. Lavric, and E. Coca, "VLC for vehicular communications: A multiple input multiple output (MIMO) approach," in *Proc. Int. Conf. Develop. Appl. Syst. (DAS)*, May 2018, pp. 134–137.

[13] T. Nawaz, M. Seminara, S. Caputo, L. Mucchi, and J. Catani, "Low-latency VLC system with Fresnel receiver for I2V ITS applications," *J. Sensor Actuator Netw.*, vol. 9, no. 3, p. 35, Jul. 2020.

[14] S. Caputo, L. Mucchi, F. Cataliotti, M. Seminara, T. Nawaz, and J. Catani, "Measurement-based VLC channel characterization for I2V communications in a real urban scenario," *Veh. Commun.*, vol. 28, Apr. 2021, Art. no. 100305.

[15] M. Elamassie, M. Karbalayghareh, F. Miramirkhani, R. C. Kizilirmak, and M. Uysal, "Effect of fog and rain on the performance of vehicular visible light communications," in *Proc. IEEE 87th Veh. Technol. Conf. (VTC Spring)*, Jun. 2018, pp. 1–6.

[16] H. B. Eldeeb, E. Eso, M. Uysal, Z. Ghassemlooy, S. Zvanovec, and J. Sathian, "Vehicular visible light communications: The impact of taillight radiation pattern," in *Proc. IEEE Photon. Conf. (IPC)*, Sep. 2020, pp. 1–2.

[17] H. B. Eldeeb, E. Eso, E. A. Jarchlo, S. Zvanovec, M. Uysal, Z. Ghassemlooy, and J. Sathian, "Vehicular VLC: A ray tracing study based on measured radiation patterns of commercial taillights," *IEEE Photon. Technol. Lett.*, early access, Mar. 10, 2021, doi: 10.1109/LPT.2021.3065233.

[18] W. Viriyasitavat, S.-H. Yu, and H.-M. Tsai, "Short paper: Channel model for visible light communications using off-the-shelf scooter taillight," in *Proc. IEEE Veh. Netw. Conf.*, Dec. 2013, pp. 170–173.

[19] M. Karbalayghareh, F. Miramirkhani, H. B. Eldeeb, R. C. Kizilirmak, S. M. Sait, and M. Uysal, "Channel modelling and performance limits of vehicular visible light communication systems," *IEEE Trans. Veh. Technol.*, vol. 69, no. 7, pp. 6891–6901, Jul. 2020.
[20] A.-L. Chen, H.-P. Wu, Y.-L. Wei, and H.-M. Tsai, "Time variation in vehicle-to-vehicle visible light communication channels," in *Proc. IEEE Veh. Netw. Conf. (VNC)*, Dec. 2016, pp. 1–8.
[21] P. Luo, Z. Ghassemlooy, H. L. Minh, E. Bentley, A. Burton, and X. Tang, "Performance analysis of a car-to-car visible light communication system," *Appl. Opt.*, vol. 54, no. 7, pp. 1696–1706, Mar. 2015.
[22] B. Aly, M. Elamassie, H. B. Eldeeb, and M. Uysal, "Experimental investigation of lens combinations on the performance of vehicular VLC," in *Proc. 12th Int. Symp. Commun. Syst., Netw. Digit. Signal Process. (CSNDSP)*, Jul. 2020, pp. 1–5.
[23] A. Al-Kinani, C.-X. Wang, Q. Zhu, Y. Fu, E.-H.-M. Aggoune, A. Talib, and N. A. Al-Hasaani, "A 3D non-stationary GBSM for vehicular visible light communication MISO channels," *IEEE Access*, vol. 8, pp. 140333–140347, 2020.
[24] A. Memedi, C. Tebruegge, J. Jahneke, and F. Dressler, "Impact of vehicle type and headlight characteristics on vehicular VLC performance," in *Proc. IEEE Veh. Netw. Conf. (VNC)*, Dec. 2018, pp. 1–8.
[25] H. B. Eldeeb, F. Miramirkhani, and M. Uysal, "A path loss model for vehicle-to-vehicle visible light communications," in *Proc. 15th Int. Conf. Telecommun. (ConTEL)*, Jul. 2019, pp. 1–5.
[26] Y. Wang, X. Huang, J. Shi, Y.-Q. Wang, and N. Chi, "Long-range high-speed visible light communication system over 100-m outdoor transmission utilizing receiver diversity technology," *Opt. Eng.*, vol. 55, no. 5, May 2016, Art. no. 056104.
[27] H. B. Eldeeb, E. Yanmaz, and M. Uysal, "MAC layer performance of multi-hop vehicular VLC networks with CSMA/CA," in *Proc. 12th Int. Symp. Commun. Syst., Netw. Digit. Signal Process. (CSNDSP)*, Jul. 2020, pp. 1–6.
[28] A. Memedi, H.-M. Tsai, and F. Dressler, "Impact of realistic light radiation pattern on vehicular visible light communication," in *Proc. IEEE Global Commun. Conf. (GLOBECOM)*, Dec. 2017, pp. 1–6.
[29] Z. Cui, P. Yue, X. Yi, and J. Li, "Research on non-uniform dynamic vehicle-mounted VLC with receiver spatial and angular diversity," in *Proc. IEEE Int. Conf. Commun. (ICC)*, May 2019, pp. 1–7.
[30] M. Morales-Cespedes, A. A. Quidan, and A. G. Armada, "Experimental evaluation of the reconfigurable photodetector for blind interference alignment in visible light communications," in *Proc. 27th Eur. Signal Process. Conf. (EUSIPCO)*, Sep. 2019, pp. 1–5.
[31] H. B. Eldeeb and M. Uysal, "Vehicle-to-vehicle visible light communication: How to select receiver locations for optimal performance?" in *Proc. 11th Int. Conf. Electr. Electron. Eng. (ELECO)*, Nov. 2019, pp. 402–405.
[32] N. Kumar, D. Terra, N. Lourenco, L. N. Alves, and R. L. Aguiar, "Visible light communication for intelligent transportation in road safety applications," in *Proc. 7th Int. Wireless Commun. Mobile Comput. Conf.*, Jul. 2011, pp. 1513–1518.
[33] K. Cui, G. Chen, Z. Xu, and R. D. Roberts, "Traffic light to vehicle visible light communication channel characterization," *Appl. Opt.*, vol. 51, no. 27, pp. 6594–6605, 2012.
[34] J.-H. Lee and S.-Y. Jung, "SNR analyses of the multi-spectral light channels for optical wireless LED communications in intelligent transportation system," in *Proc. IEEE 79th Veh. Technol. Conf. (VTC Spring)*, May 2014, pp. 1–5.
[35] T. Nawaz, M. Seminara, S. Caputo, L. Mucchi, F. S. Cataliotti, and J. Catani, "IEEE 802.15. 7-compliant ultra-low latency relaying VLC system for safety-critical ITS," *IEEE Trans. Veh. Technol.*, vol. 68, no. 12, pp. 12040–12051, Oct. 2019.
[36] M. Seminara, T. Nawaz, S. Caputo, L. Mucchi, and J. Catani, "Characterization of field of view in visible light communication systems for intelligent transportation systems," *IEEE Photon. J.*, vol. 12, no. 4, pp. 1–16, Aug. 2020.
[37] X. You, Y. Zhong, J. Chen, and C. Yu, "Mobile channel estimation based on decision feedback in vehicle-to-infrastructure visible light communication systems," *Opt. Commun.*, vol. 462, May 2020, Art. no. 125261.
[38] M. S. Demir, H. B. Eldeeb, and M. Uysal, "CoMP-based dynamic handover for vehicular VLC networks," *IEEE Commun. Lett.*, vol. 24, no. 9, pp. 2024–2028, Sep. 2020.
[39] M. A. Vieira, M. Vieira, P. Louro, and P. Vieira, "Redesign of the trajectory within a complex intersection for visible light communication ready connected cars," *Opt. Eng.*, vol. 59, no. 9, Sep. 2020, Art. no. 097104.
[40] M. A. Vieira, M. Vieira, P. Louro, and P. Vieira, "Cooperative vehicular communication systems based on visible light communication," *Opt. Eng.*, vol. 57, no. 7, Jul. 2018, Art. no. 076101.
[41] M. W. Hancock and B. Wright, "A policy on geometric design of highways and streets," Amer. Assoc. State Highway Transp. Officials, Washington, DC, USA, Tech. Rep. 990, 2013.
[42] F. Miramirkhani and M. Uysal, "Channel modeling and characterization for visible light communications," *IEEE Photon. J.*, vol. 7, no. 6, pp. 1–16, Dec. 2015.
[43] Z. N. Chaleshtori, S. Zvanovec, Z. Ghassemlooy, H. B. Eldeeb, and M. Uysal, "Coverage of a shopping mall with flexible OLED-based visible light communications," *Opt. Exp.*, vol. 28, no. 7, pp. 10015–10026, 2020.
[44] M. Uysal, F. Miramirkhani, O. Narmanlioglu, T. Baykas, and E. Panayirci, "IEEE 802.15.7r1 reference channel models for visible light communications," *IEEE Commun. Mag.*, vol. 55, no. 1, pp. 212–217, Jan. 2017.
[45] H. B. Eldeeb, M. Uysal, S. M. Mana, P. Hellwig, J. Hilt, and V. Jungnickel, "Channel modelling for light communications: Validation of ray tracing by measurements," in *Proc. 12th Int. Symp. Commun. Syst., Netw. Digit. Signal Process. (CSNDSP)*, Jul. 2020, pp. 1–6.
[46] H. B. Eldeeb, S. M. Mana, V. Jungnickel, P. Hellwig, J. Hilt, and M. Uysal, "Distributed MIMO for Li-Fi: Channel measurements, ray tracing and throughput analysis," *IEEE Photon. Technol. Lett.*, early access, Apr. 9, 2021, doi: 10.1109/LPT.2021.3072254.
[47] H. B. Eldeeb, M. Elamassie, and M. Uysal, "Vehicle-to-infrastructure visible light communications: Channel modelling and capacity calculations," in *Proc. 12th Int. Symp. Commun. Syst., Netw. Digit. Signal Process. (CSNDSP)*, Jul. 2020, pp. 1–6.
[48] Z. Ghassemlooy, W. Popoola, and S. Rajbhandari, *Optical Wireless Communications: System and Channel Modelling With MATLAB*. Boca Raton, FL, USA: CRC Press, 2019.
[49] *LUXEON Rebel Automotive*. Accessed: Feb. 20, 2021. [Online]. Available: https://www.lumileds.com/products/automotive-lighting/luxeon-rebel-automotive/
[50] *OSRAM Vehicular Light Sources*. Accessed: Jul. 24, 2021. [Online]. Available: https://www.osram.com/os/products/product-promotions/
[51] *Vestel Streetlight Sources*. Accessed: Jul. 24, 2021. [Online]. Available: https://www.vestelledlighting.com/eu-en/ephesus-m4s-68
[52] S.-H. You, S.-H. Chang, H.-M. Lin, and H.-M. Tsai, "Visible light communications for scooter safety," in *Proc. 11th Annu. Int. Conf. Mobile Syst., Appl., Services (MobiSys)*, 2013, pp. 509–510.
[53] R. Zhang, M. Biagi, L. Lampe, T. D. C. Little, S. Mangold, and Z. Xu, "Guest editorial localisation, communication and networking with VLC," *IEEE J. Sel. Areas Commun.*, vol. 36, no. 1, pp. 1–7, Jan. 2018.
[54] O. Narmanlioglu, B. Turan, B. Kebapci, S. C. Ergen, and M. Uysal, "Poster: On-board camera video transmission over vehicular VLC," in *Proc. IEEE Veh. Netw. Conf. (VNC)*, Dec. 2016, pp. 1–2.

HOSSIEN B. ELDEEB (Graduate Student Member, IEEE) received the B.Sc. degree (Hons.) in electronics and electrical communication engineering from Menoufia University, Minuf, Egypt, in 2008, and the M.Sc. degree in electrical and electronics communication engineering from Cairo University, Cairo, Egypt, in 2017. He is currently pursuing the Ph.D. degree with the Communication Theory and Technologies (CT&T) Research Group, Özyeğin University, Istanbul, Turkey, under the supervision of Prof. Murat Uysal. He joined the CT&T Research Group as a Research Assistant, in 2018. He is also working as a Research Engineer with EU-ITN-Vision Project. He has practical experience, having served as an Instrumentation and Control Engineer and a Operation Engineer for the Cairo-West and Giza-North Electrical Power Stations, Giza, Egypt. His current research interests include photonics and optical wireless communications, channel modeling for indoor and outdoor visible light communications, optical system design, ray tracing, channel measurements for light communication systems, combining schemes, and diversity techniques. He is a member of Institute of the Electrical & Electronics Engineers (IEEE) Society and IEEE Photonics Society. He received the Best Paper Award from the IEEE/IET CSNDSP 2020. He contributed at the upcoming IEEE Standard IEEE-802-11-TGbb.

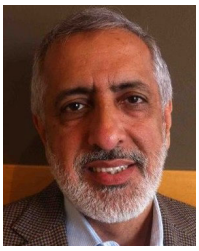

SADIQ M. SAIT (Senior Member, IEEE) was born in Bengaluru. He received the bachelor's degree in electronics engineering from Bangalore University, in 1981, and the master's and Ph.D. degrees in electrical engineering from King Fahd University of Petroleum and Minerals (KFUPM), in 1983 and 1987, respectively. He is currently a Professor of computer engineering and the Director of the Center for Communications and IT Research, Research Institute, KFUPM. He has authored over 200 research articles, contributed chapters to technical books, and granted several U.S. patents. He has lectured over 30 countries. He is also the Principle Author of two books (published by McGraw Hill Book Company, IEEE, the IEEE Computer Society Press, and the World Scientific). He received the Best Electronic Engineer Award from the Indian Institute of Electrical Engineers, Bengaluru, in 1981, and several other awards during the course of his career.

MURAT UYSAL (Fellow, IEEE) received the B.Sc. and M.Sc. degrees in electronics and communication engineering from Istanbul Technical University, Istanbul, Turkey, in 1995 and 1998, respectively, and the Ph.D. degree in electrical engineering from Texas A&M University, College Station, TX, in 2001.

He is currently a Full Professor and the Chair of the Department of Electrical and Electronics Engineering at Özyeğin University, Istanbul. He also serves as the Founding Director of the Center of Excellence in Optical Wireless Communication Technologies (OKATEM). Prior to joining Özyeğin University, he was a tenured Associate Professor at the University of Waterloo, Canada. His research interests include communication theory, with a particular emphasis on the physical layer aspects of wireless communication systems in radio and optical frequency bands. On these topics, he has authored around 400 journals and conference papers and received more than 15 000 citations with an H-index of 58.

Prof. Uysal was a recipient of the NSERC Discovery Accelerator Award, in 2008; the University of Waterloo Engineering Research Excellence Award, in 2010; the Turkish Academy of Sciences Distinguished Young Scientist Award, in 2011; the Özyeğin University Best Researcher Award, in 2014; the National Instruments Engineering Impact Award, in 2017; the Elginkan Foundation Technology Award, in 2018; and the IEEE Communications Society Best Survey Paper Award, in 2019. He is the former Chair of IEEE Turkey Section. He was involved in the organization of several IEEE conferences at various levels. In particular, he served as the Technical Program Committee Chair of major IEEE conferences, including WCNC 2014, PIMRC 2019, and VTC-Fall 2019. He currently serves on the Editorial Board of IEEE TRANSACTIONS ON WIRELESS COMMUNICATIONS. In the past, he served as an Editor for IEEE TRANSACTIONS ON COMMUNICATIONS, IEEE TRANSACTIONS ON VEHICULAR TECHNOLOGY, and IEEE COMMUNICATIONS LETTERS.